SUPPLEMENTAL INFORMATION

SUPPLEMENTAL METHODS

Isolation of Mouse Embryonic Dermal LECs

Embryo back skins with proper genotypes were harvested, chopped into small pieces, and then treated with dispase and collagenase (1mg/mL, Hoffmann-La Roche, Ltd), collagenase II (50 U/mL, Worthington Biochemical, Lakewood, NJ) and DNase I (1,000 U/mL, New England Biolabs, Ipswich, MA) in phosphate buffered saline (PBS) at 37 °C for 1 hr. Dermal cell mixtures were isolated by triturating enzymatically treated back skins through a needle (18.5G) and filtering through a cell strainer. Cells were then centrifuged, resuspended in EBM-based media, seeded on a culture dish, and incubated 37 °C for 4 hr. The cultures were washed with PBS twice, trypsinized, and then incubated with LYVE1 antibody (Angiobio, 11-034) at 4 °C for 1 hr. Concurrently, biotinylated goat anti-rabbit IgG antibody (Vector Laboratories, BA-1000) and Dynabeads Biotin Binder (Invitrogen, 11047) were separately incubated at 4 °C for 1 hr. and then finally mixed with the cells incubated with the LYVE1 antibody at 4 °C for 1 hr., followed by RNA isolation processes using Trizol solution (Thermo Fisher Scientific).

Gene and Protein Expression, Plasmids and Vectors, Mutagenesis

Standard protocols were employed for quantitative real-time RT-PCR and western blotting. Plasmids and siRNAs were transfected into target cells using HMEC-L Nucleofector Kit (Lonza, VPB1003) or PBS (1), respectively. Immunofluorescent staining for whole-mount/tissue sections was performed as previously described (2). Sources of expression vectors are as follows: Myc-tag PROX1 (Dr. Paul A. Overbeek, Baylor College of Medicine, Houston, TX) (3), FLAG-tag KLF2 (Dr. Hiroaki Taniguchi, University of Tokyo, Tokyo, Japan) (4), Myc-tag DTX1 and HA-tag DTX3L (Dr. Margaret A. Shipp, Harvard Medical School, Boston, MA) (5), and pGa981-6/TP1-luc (Dr. Hua Han, Fourth Military Medical University, Xi'an, China) (6). The following are the vectors that were generated for this study: For pcDNA3-HA-CaM (YH2307), human CaM fragment was constructed by PCR using a EcoRV site-containing forward primer and a XhoI site-harboring reverse primer, and cloned into EcoRV/XhoI sites of pcDNA3 (Life Technologies). The primer sequences are listed in Supplemental Table2. We constructed recombinant GST-PROX1 fusion

vectors as follows. Human PROX1 fragment (1-546 a.a.) was PCR-amplified from a human cDNA library using a primer set (Supplemental Table2) and cloned in EcoRI/SalI sites of pGEX-5X-1. The resulting vector (YH2012) was digested with EcoRI/SmaI and the insert was transferred to EcoRI/SmaI sites of pGEX-5X-1 to generate PROX1-D1 (YH2722). For PROX1-D2 to PROX1-D7, PROX1 fragments were PCR-amplified against human PROX1 cDNA with forward and reverse primers harboring a EcoRI site and a SalI site, respectively, and cloned into EcoRI/SalI sites of pGEX-5X-1 (GE Healthcare Life Sciences). Their sequences are listed in Supplemental Table2. These GST-PROX1 fusion vectors were transformed into BL21 bacterial strain and recombinant GST-PROX1 fusion fragments were produced and purified as described previously (7). For Dtx3L-transgenic vector (YH3004), mouse Dtx3L was PCR-amplified from pCR4-TOPO-mDtx3L (Source Bioscience, Santa Fe Springs, CA) and cloned into NotI/EcoRI site of pcDNA3. The resulting construct was then PCR-amplified, digested with BamHI and PacI and cloned into BglII/PacI sites of a *LoxP*-Stop-*LoxP*-containing conditional expression vector, pCAG-sGFP-4X L2 Pac (kindly provided by Dr. Jeong K. Yoon, Maine Medical Center Research Institute, Scarborough, ME) (8). Substitution mutagenesis to aspartic acid (D) in human PROX1 protein was performed using corresponding mutagenesis primers as previously described (9). Sequences of all the primers are listed in Supplemental Table2.

Notch Activity Reporter Assay

Human primary LECs were transfected with a RBP-JK reporter luciferase vector, pGa981-6/TP1-luc (6), or the parental vector (pGL3-Basic, Promega Corporation, Madison, WI) for 24 hr. The cells were then subjected to steady laminar flow at 2 dyne/cm^2 for 24 or 48 hr., followed by a standard luciferase assay using Bright-Glo™ Luciferase Assay System (Promega). Total cell lysate was quantified by the Bradford assay (Sigma-Aldrich) and equal amount of the lysates was used for the luciferase assay.

Confocal Laser-Scanning Fluorescence Microscopy for Calcium Imaging

Primary LECs were seeded and preloaded with Fluo-4 on μ-Slides and unidirectional laminar flow (2 dyne/cm^2) was applied using a pump that was connected to the slide. Calcium releasing signals were

captured with a Leica TCS SP5 AOTF MP confocal microscope system (Leica Microsystems, Heidelberg, Germany). A Leica DMI6000 inverted microscope with 20X 0.7NA objective (Leica Microsystems) was powered by an Argon 488-nm for these studies. Images were collected in time series (*xyt*, 1 s per frame) with the Leica LAS AF imaging software, and excitation at 488 nm, emission at 520 ± 50 nm was used. All experiments were performed with the same instrument settings (laser power, offset, gain of both detector channels). Fluorescence intensity (8 bit) was measured with the Leica LAS lite imaging software's Quantification Tools.

CaM Overlay Assay

CaM overlay assays were performed to determine *in vitro* protein-protein interaction between PROX1 protein fragments and HRP-conjugated CaM protein on western membranes. Western blotting assay was first performed to detect the quantity and quality of GST-PROX1 fusion fragments that were produced in bacteria (top panel, Fig.4A). CaM overlay assays were then performed as previously described (7). Briefly, duplicate GST-PROX1 fragment blots were probed with GmCaM1::HRP and GmCaM4::HRP conjugates in the presence of $CaCl_2$ (1 mM) or EGTA (5 mM) (middle and bottom panels, respectively, Fig.4A). The bound HRP-conjugated CaM protein was visualized using ECL detection system (GE Healthcare Life Sciences).

NMR Study

The NMR sample contained 0.5 mM ^{15}N-labeled CaM, 100 mM KCl, 20 mM Bis-Tris (pH 6.8), 5 mM $CaCl_2$, 0.5 mM 2,2-dimethyl-2-silapentane-5-sulfonate (DSS) in 10%D_2O/90%H_2O. A stock solution of 5 mM PROX1 peptide in the same buffer was titrated into the NMR sample. The titration was monitored through HSQC experiments acquired on a Bruker Avance 700 MHz NMR spectrometer at 30 °C. DSS was used as a reference to obtain the ^{1}H and ^{15}N chemical shifts. The spectra were processed with NMRPipe (10) and analyzed using NMRView (11). The chemical shift assignment for Ca^{2+}-CaM was obtained from Gifford *et al* (11).

Co-Immunoprecipitation

The standard co-immunoprecipitation protocol was used to show a direct protein-protein interaction as previously described (12). For the serial co-IP, plasmid vectors expressing Myc-PROX1 and HA-CaM were co-transfected in HEK293 cells with or without a FLAG-KLF2-expressing vector for 48 hr. Cell were lysed in PBS containing NP-40 (0.5%) to harvest whole cell lysates (WCL), which were then incubated with FLAG-antibody beads to precipitate KLF2 by centrifugation at 4 °C. The KLF2-containing precipitants were eluted into the same lysis buffer (PBS with NP-40, 0.5%) from the FLAG-beads using FLAG peptide (0.5 mg/mL, LifeTein, LLC). Elutes from the KLF2-expressing cell lysates (+KLF2) were again precipitated using normal IgG or anti-HA antibody, followed by incubation with Protein-A/G beads (Pierce) to precipitate HA-CaM. The resulting isolates from both rounds of co-IPs were blotted with anti-FLAG, anti-HA, and anti-Myc antibodies.

3-D Microfluidic Sprouting Assay

A microfluidic device was used to assemble vessel-like structures that are lined with BECs or LECs as described previously (13). Briefly, collagen 1 (2.5 mg/mL) was polymerized in the device around two 400-μm-diameter needles. After removing the needles, BECs or LECs were seeded (4 million/mL) into one channel, and we allowed them to form a confluent monolayer overnight. Devices were placed on a platform rocker to generate gravity-driven flow (5 dyne/cm^2) or placed on a static incubator. Growth factors were added to the opposite channel to induce sprouting as described previously (13).

Supplemental References

1. Kang, J., Ramu, S., Lee, S., Aguilar, B., Ganesan, S.K., Yoo, J., Kalra, V.K., Koh, C.J., and Hong, Y.K. 2009. Phosphate-buffered saline-based nucleofection of primary endothelial cells. *Anal Biochem* 386:251-255.

2. Choi, I., Chung, H.K., Ramu, S., Lee, H.N., Kim, K.E., Lee, S., Yoo, J., Choi, D., Lee, Y.S., Aguilar, B., et al. 2011. Visualization of lymphatic vessels by Prox1-promoter directed GFP reporter in a bacterial artificial chromosome-based transgenic mouse. *Blood* 117:362-365.

3. Chen, Q., Dowhan, D.H., Liang, D., Moore, D.D., and Overbeek, P.A. 2002. CREB-binding protein/p300 co-activation of crystallin gene expression. *J Biol Chem* 277:24081-24089.

4. Taniguchi, H., Jacinto, F.V., Villanueva, A., Fernandez, A.F., Yamamoto, H., Carmona, F.J., Puertas, S., Marquez, V.E., Shinomura, Y., Imai, K., et al. 2012. Silencing of Kruppel-like factor 2 by the histone methyltransferase EZH2 in human cancer. *Oncogene* 31:1988-1994.

5. Takeyama, K., Aguiar, R.C., Gu, L., He, C., Freeman, G.J., Kutok, J.L., Aster, J.C., and Shipp, M.A. 2003. The BAL-binding protein BBAP and related Deltex family members exhibit ubiquitin-protein isopeptide ligase activity. *J Biol Chem* 278:21930-21937.

6. Minoguchi, S., Taniguchi, Y., Kato, H., Okazaki, T., Strobl, L.J., Zimber-Strobl, U., Bornkamm, G.W., and Honjo, T. 1997. RBP-L, a transcription factor related to RBP-Jkappa. *Mol Cell Biol* 17:2679-2687.

7. Yoo, J.H., Cheong, M.S., Park, C.Y., Moon, B.C., Kim, M.C., Kang, Y.H., Park, H.C., Choi, M.S., Lee, J.H., Jung, W.Y., et al. 2004. Regulation of the dual specificity protein phosphatase, DsPTP1, through interactions with calmodulin. *J Biol Chem* 279:848-858.

8. Venkatesh, D.A., Park, K.S., Harrington, A., Miceli-Libby, L., Yoon, J.K., and Liaw, L. 2008. Cardiovascular and hematopoietic defects associated with Notch1 activation in embryonic Tie2-expressing populations. *Circ Res* 103:423-431.

9. Kunkel, T.A. 1985. Rapid and efficient site-specific mutagenesis without phenotypic selection. *Proc Natl Acad Sci U S A* 82:488-492.

10. Delaglio, F., Grzesiek, S., Vuister, G.W., Zhu, G., Pfeifer, J., and Bax, A. 1995. NMRPipe: a multidimensional spectral processing system based on UNIX pipes. *J Biomol NMR* 6:277-293.

11. Johnson, B.A. 2004. Using NMRView to visualize and analyze the NMR spectra of macromolecules. *Methods Mol Biol* 278:313-352.

12. Choi, I., Lee, S., Kyoung Chung, H., Suk Lee, Y., Eui Kim, K., Choi, D., Park, E.K., Yang, D., Ecoiffier, T., Monahan, J., et al. 2012. 9-cis retinoic Acid promotes lymphangiogenesis and enhances lymphatic vessel regeneration: therapeutic implications of 9-cis retinoic Acid for secondary lymphedema. *Circulation* 125:872-882.

13. Nguyen, D.H., Stapleton, S.C., Yang, M.T., Cha, S.S., Choi, C.K., Galie, P.A., and Chen, C.S. 2013. Biomimetic model to reconstitute angiogenic sprouting morphogenesis in vitro. *Proc Natl Acad Sci U S A* 110:6712-6717.

SUPPLEMENTAL FIGURE LEGENDS

Supplemental Figure 1. Laminar flow selectively suppresses NOTCH1 activity in LECs

(**A**) Cell morphology of LECs and BECs in response to low-rate steady laminar flow (LF) at 2 dyne/cm^2 for 0 (static), 12, 24, and 48 hr. Scale bars: 50 μm.

(**B-D**) Real-time RT-PCR (qRT-PCR) data showing the mRNA levels of eNOS in LECs and BECs (**B**), Notch target genes in BECs (**C**), and NOTCH1 in LECs (**D**) in response to steady laminar flow at 2 dyne/cm^2 for the indicated time.

(**E**) Western blot bands of NICD-1 in Fig.1C in the main text were quantitated and charted.

(**F,G**) Protein levels (**F**) and their band intensity (**G**) of NICD-4 in LECs and BECs in response to laminar flow at 2 dyne/cm^2 for the indicated time.

(**H**) Prox1 protein level was not altered in LECs that were exposed to laminar flow (2 dyne/cm^2).

(**I**) The biomimetic sprouting assay shown in Fig.1F was performed on BECs. Intraluminal laminar flow (5 dyne/cm^2) was applied onto a layer of BECs lining the inner wall of the vascular-mimetic channels made in collagen gel. Scale bars: 100 μm. Relative sprout number and length were graphed.

Error bars represent standard deviation (SD). Statistical values: n.s., not significant; *, $p < 0.05$; **, $p < 0.01$; ***, $p < 0.001$.

Supplemental Figure 2. Quantitation of the effect of siRNA-mediated knockdown of ORAI1. Intensity of NICD-1 bands in LECs (**A**) and BECs (**B**) after siRNA-mediated knockdown of ORAI1 shown in Fig.2C was quantified and charted. (**C**) Laminar flow-induced calcium influx was measured in LECs transfected with either scrambled siRNA (siCTR) or ORAI1 siRNA (siOrai1) for 24 hr., followed by laminar flow (2 dyne/cm^2). Calcium signals were captured by a time-lapse microscope and the relative signal intensity was plotted. Error bars represent standard deviation (SD). Statistical values: **, $p < 0.01$; ***, $p < 0.001$.

Supplemental Figure 3. Defective lymphatic development in Orai1 KO embryo. (A-H) Low magnification images of the Cd31/Lyve1-stained back skins of Orai1 wild type (+/+) and KO (-/-) embryos

(E15.5). Two sets (#1 and #2) of wild type (**A-D**) and KO (**E-H**) embryos from two different litters are shown. Scale bars: 200 μm. **(I)** Relative calibers of lymphatic vessels in Orai1 wild type vs. KO embryos. Error bars represent standard deviation (SD). Statistical values: *, $p < 0.05$; **, $p < 0.01$; ***, $p < 0.001$

Supplemental Figure 4. Sequence-based prediction of a putative CaM-binding site in the N-terminus of PROX1 (**A**) A potential CaM binding site was identified in the N-terminal area of PROX1 by the Camodulin Target Database Binding Site Search algorithm, established by the Mitsu Ikura Lab (Ontario Cancer Institute, Canada). Probability scores (from 0 to 9) were shown below each amino acid residue. The putative CaM binding site mapped between 5^{th} and 37^{th} amino acid in PROX1 is underlined. (**B**) Diagram of GST-PROX1 fragments. The N-terminus of each PROX1 fragment was fused to GST protein (empty circle) for bacterial expression and purification. The location of each end is shown. NR, nuclear receptor binding motif; Homeo, homeodomain.

Supplemental Figure 5. Quantitation of western blot bands. Intensity of western blot bands in Figs.4 and 5 was measured, normalized and graphed. (**A**) Band intensity of Prox1 proteins that were immunoprecipitated by anti-HA antibody in Fig.4E was quantitated. (**B**) Band intensity of CaM proteins that were co-precipitated with Prox1 in Fig.4F was quantitated using the short exposure. (**C**) Band intensity of Myc-Prox1 proteins that were co-precipitated with FLAG-KLF2 in Fig.5B was quantitated. (**D**) Band intensity of Myc-Prox1 proteins that were co-precipitated with FLAG-KLF2 in the absence (Empty) or presence (HA-CaM) of CaM protein in Fig.5C was quantitated.

Supplemental Figure 6. PROX1 binds with GCamP3, but with GFP. An expression vector encoding GCaMP3 or GFP was co-transfected with a vector expressing Myc-PROX1 into HEK293 cells. After 48 hours, GFP or GCaMP3 was immunoprecipitated from the cell lysates using anti-GFP antibody or normal rabbit IgG as a negative control, which were then blotted with anti-Myc or anti-GFP antibody. Note that only GCaMP3, not GFP, was immunoprecipitated with PROX1.

Supplemental Figure 7. Nuchal edema in endothelial-specific Klf2 KO embryos. Wild type and endothelial-specific Klf2 KO embryos (Klf2 ^{ECKO}) resulted from crossing the Cdh5(PAC)-CreER^{T2} mice and Klf2 $^{fl/fl}$ mice are shown at E15.5. Two different litters are shown (#1 and #2). Klf2 ^{ECKO} was induced in pregnant females by intraperitoneal injection of tamoxifen (1.5 mg) at E11.5 and E13.5. Arrowheads mark nuchal edema. Dermal lymphatics were often filled with blood as shown in the white box.

Supplemental Figure 8. Low-power images of the back skins of wild type and Klf2 ^{ECKO} embryos of Fig.5I. Overview low-magnification images of lymphatic vessels (shown by EGFP) and blood vessels (stained with Cd31) demonstrate the vascular defects caused by genetic ablation of Klf2 in endothelial cells.

Supplemental Figure 9. Regulation of DTX1 and DTX3L protein expression in LECs *vs*. BECs by laminar flow. Western blot assays showing the regulation of protein expression of DTX1 (**A**) and DTX3L (**B**) in LECs and BECs after exposure to laminar flow (2 dyne/cm^2) for 0 (Static), 12 or 24 hr.. These protein expression data are consistent with their mRNA expression patterns shown in Fig.6 A and B, respectively.

Supplemental Figure 10. Synergistic downregulation of NICD-1 by DTX1 and DTX3L. Western blot bands for NICD-1 shown in Fig.6 E, F, and G were quantified and charted in panels **A**, **B**, and **C**, respectively. Statistical values: *, $p < 0.05$; **, $p < 0.01$; ***, $p < 0.001$.

Supplemental Figure 11. Low-power images of the back skins of wild type *vs.* Dtx3L knockout embryos. Overview low-magnification images for Lyve1 show defective lymphatic sprouting in Dtx3L KO embryos at E15.5. Total > 4 embryos per genotype harvested from at least 3 independent litters were analyzed for the study.

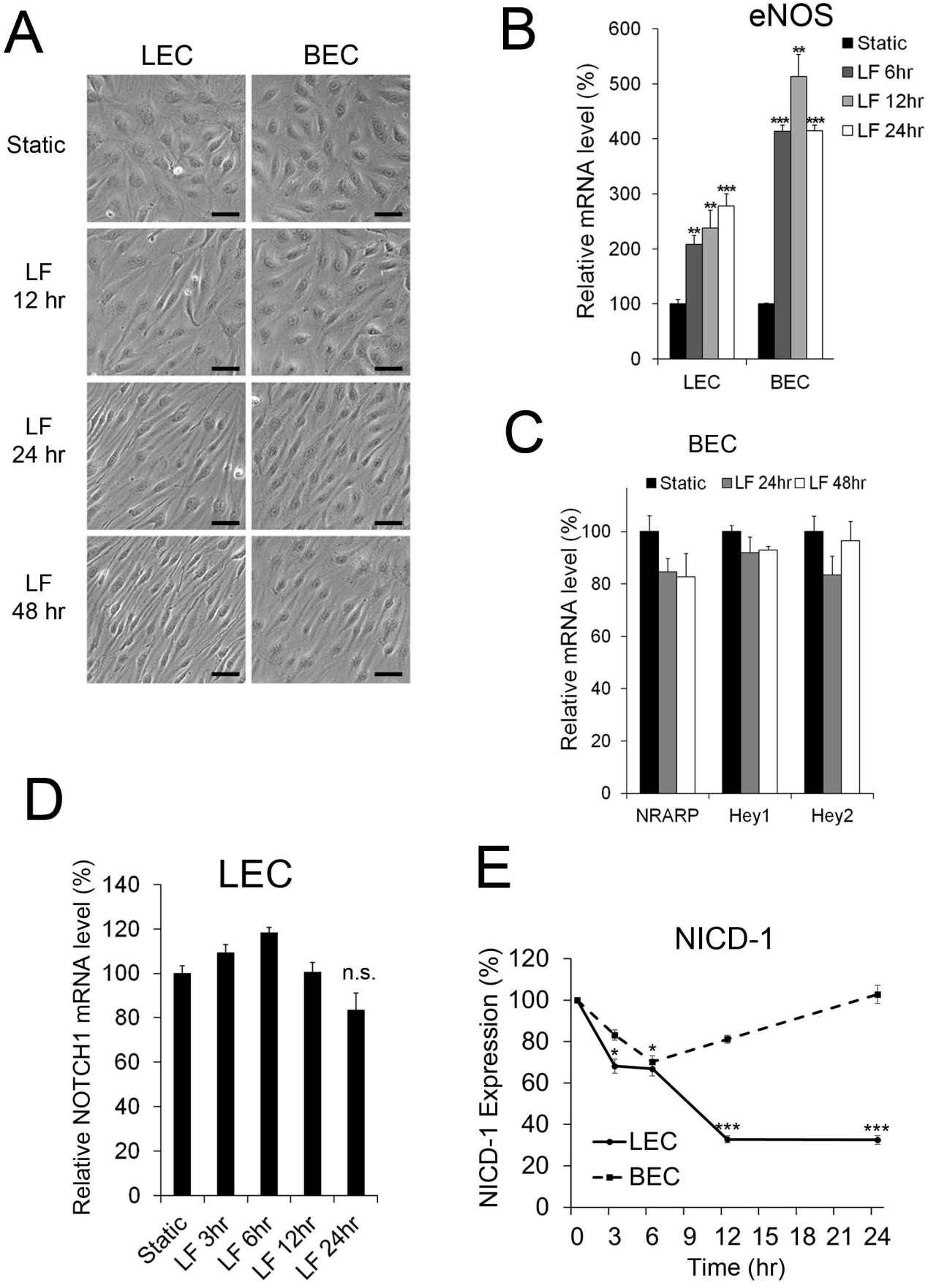

Supplemental Figure1 (Part1)

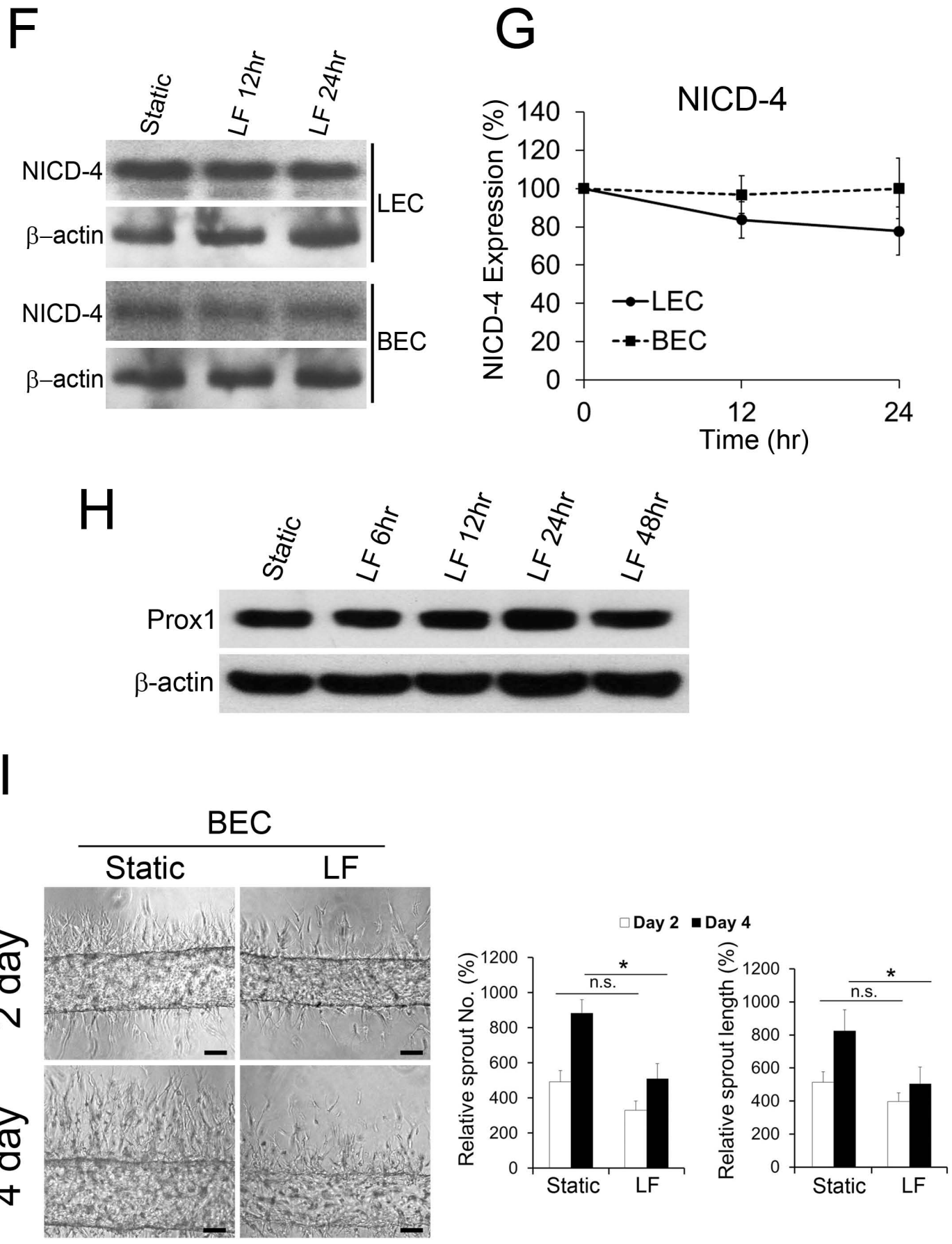

Supplemental Figure 1 (Part2)

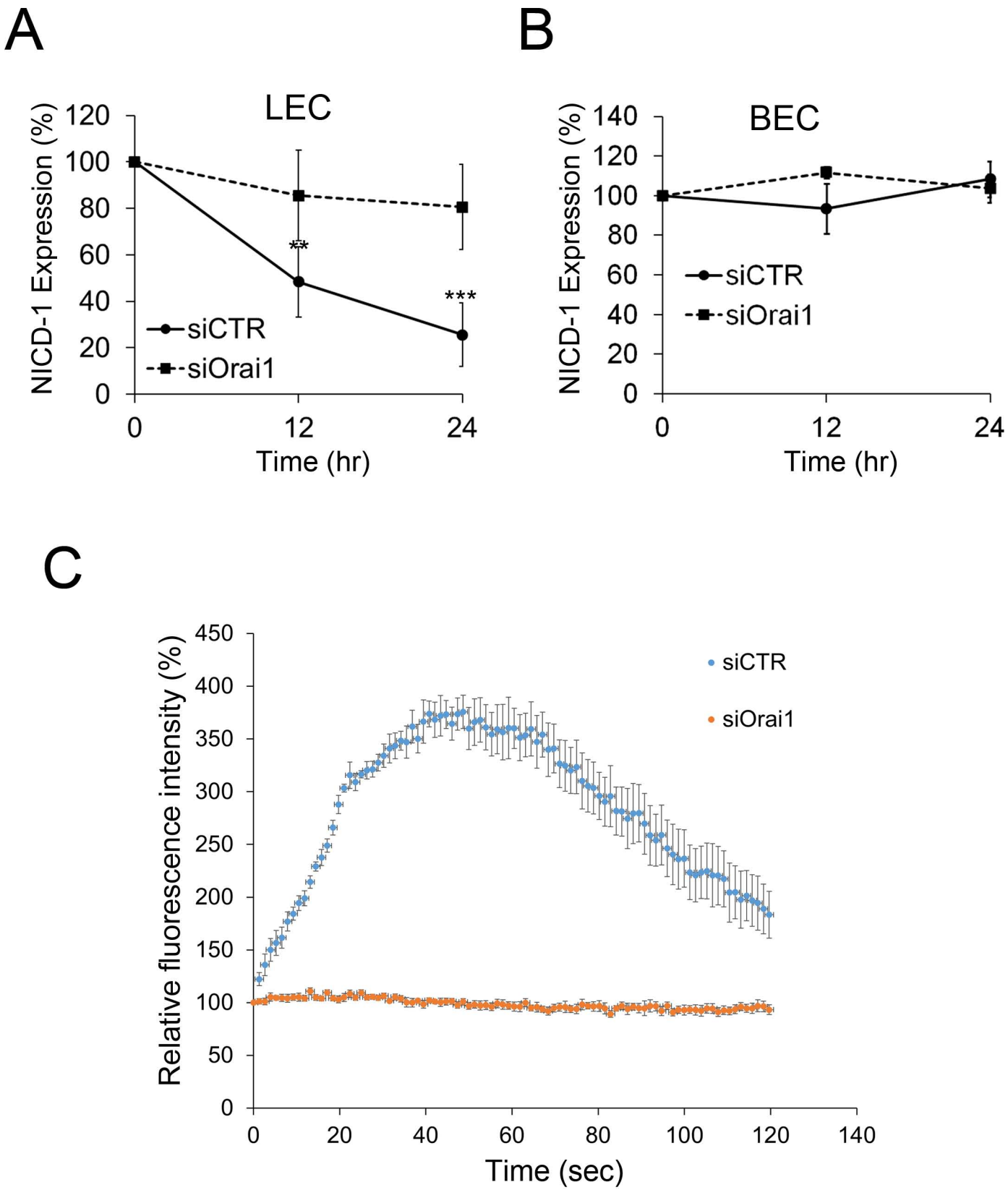

Supplemental Figure 2

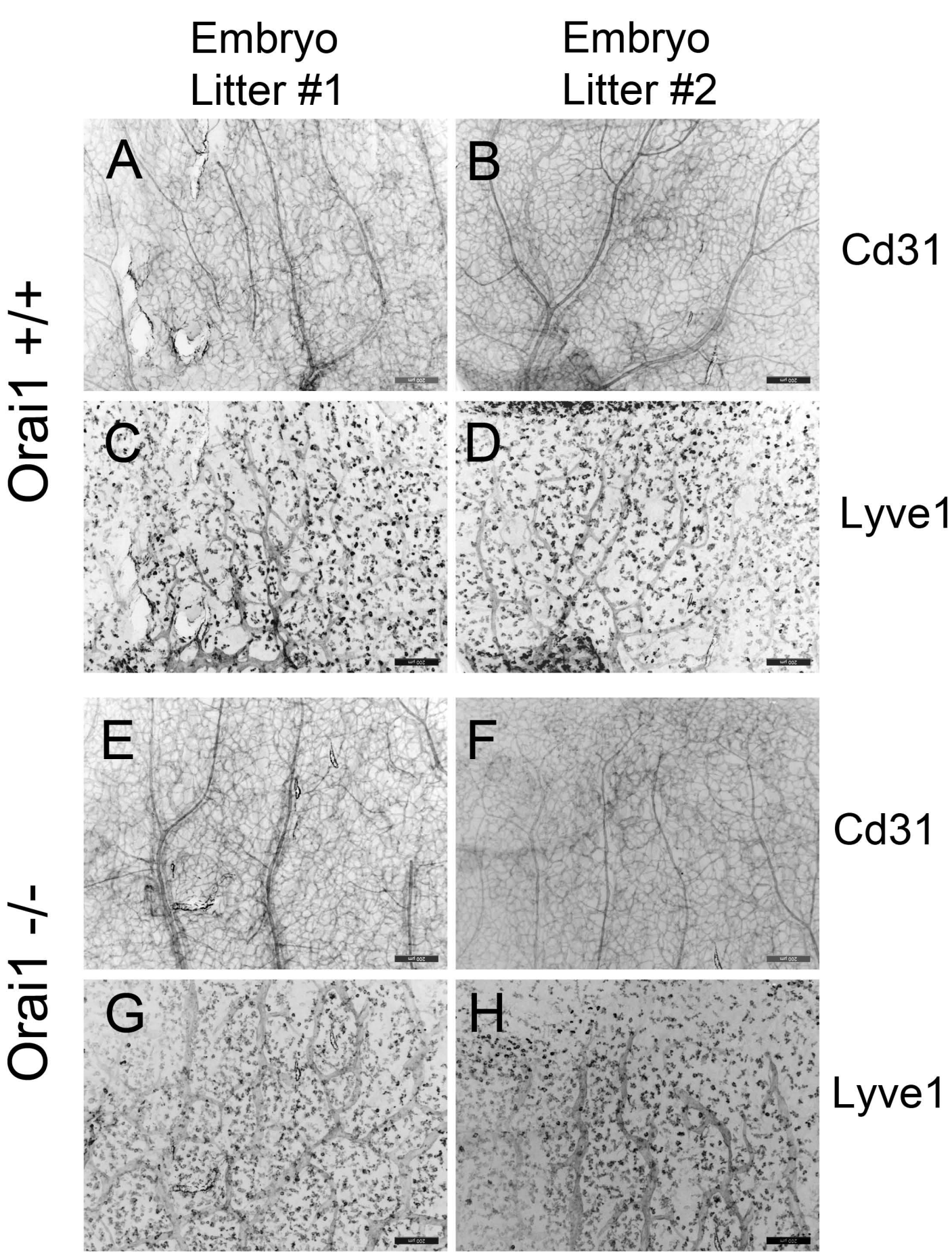

Supplemental Figure 3 (Part1)

I

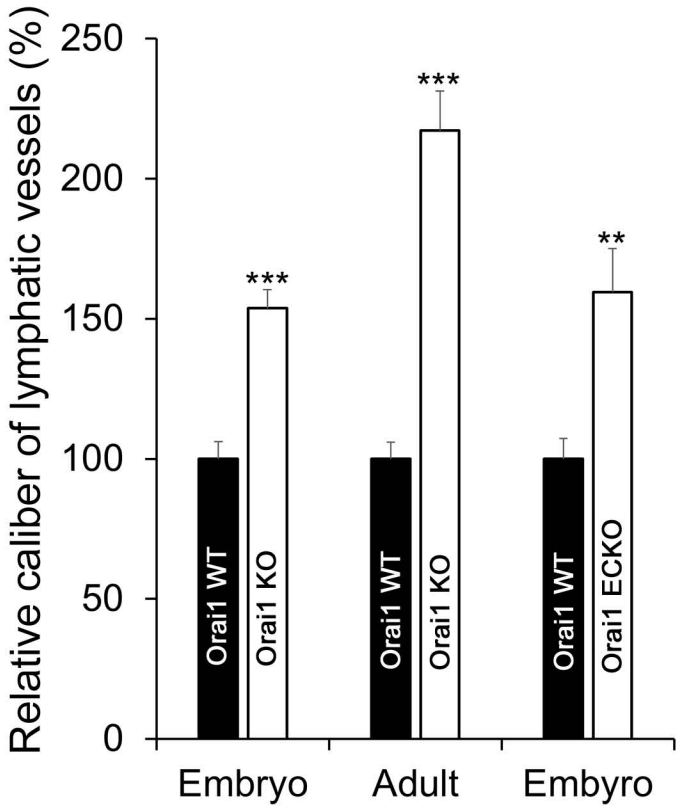

Supplemental Figure 3 (Part2)

A

```
....1 MPDHDSTALL SRQTKRRRVD IGVKRTVGTA SAFFAKARAT FFSAMNPQGS
..... 0000111233 4566789999 9999988766 5433211000 0000000000

...51 EQDVEYSVVQ HADGEKSNVL RKLLKRANSY EDAMMPFPGA TIISQLLKNN
..... 0000000000 0000000000 0000000000 0000000000 0000000000

..101 MNKNGGTEPS FQASGLSSTG SEVHQEDICS NSSRDSPPEC LSPFGRPTMS
..... 0000000000 0000000000 0000000000 0000000000 0000000000

..151 QFDMDRLCDE HLRAKRARVE NIIRGMSHSP SVALRGNENE REMAPQSVSP
..... 0000000000 0000000000 0000000000 0000000000 0000000000

..201 RESYRENKRK QKLPQQQQQS FQQLVSARKE QKREERRQLK QQLEDMQKQL
..... 0000000000 0000000000 0000000000 0000000000 0000000000

..251 RQLQEKFYQI YDSTDSENDE DGNLSEDSMR SEILDARAQD SVGRSDNEMC
..... 0000000000 0000000000 0000000000 0000000000 0000000000

..301 ELDPGQFIDR ARALIREQEM AENKPKREGN NKERDHGPNS LQPEGKHLAE
..... 0000000000 0000000000 0000000000 0000000000 0000000000

..351 TLKQELNTAM SQVVDTVVKV FSAKPSRQVP QVFPPLQIPQ ARFAVNGENH
..... 0000000000 0000000000 0000000000 0000000000 0000000000

..401 NFHTANQRLQ CFGDVIIPNP LDTFGNVQMA SSTDQTEALP LVVRKNSSDQ
..... 0000000000 0000000000 0000000000 0000000000 0000000000

..451 SASGPAAGGH HQPLHQSPLS ATTGFTTSTF RHPFPLPLMA YPFQSPLGAP
..... 0000000000 0000000000 0000000000 0000000000 0000000000

..501 SGSFSGKDRA SPESLDLTRD TTSLRTKMSS HHLSHHPCSP AHPPSTAEGL
..... 0000000000 0000000000 0000000000 0000000000 0000000000

..551 SLSLIKSECG DLQDMSEISP YSGSAMQEGL SPNHLKKAKL MFFYTRYPSS
..... 0000000000 0000000000 0000000011 1111111111 1111111100

..601 NMLKTYFSDV KFNRCITSQL IKWFSNFREF YYIQMEKYAR QAINDGVTST
..... 0000000000 0000000001 1123333333 3333333332 1110000000

..651 EELSITRDCE LYRALNMHYN KANDFEVPER FLEVAQITLR EFFNAIIAGK
..... 0000000000 0000000000 0000000000 0000000000 0000000000

..701 DVDPSWKKAI YKVICKLDSE VPEIFKSPNC LQELLHE
..... 0000000000 0000000000 0000000000 0000000
```

B

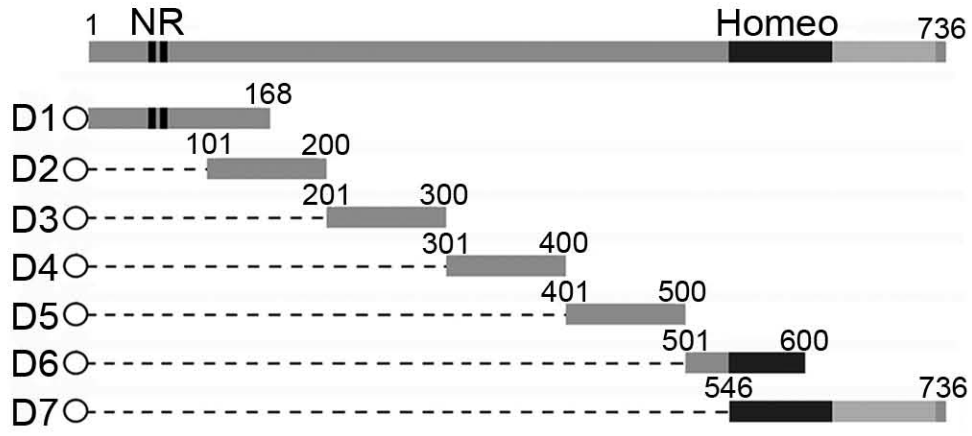

Supplemental Figure 4

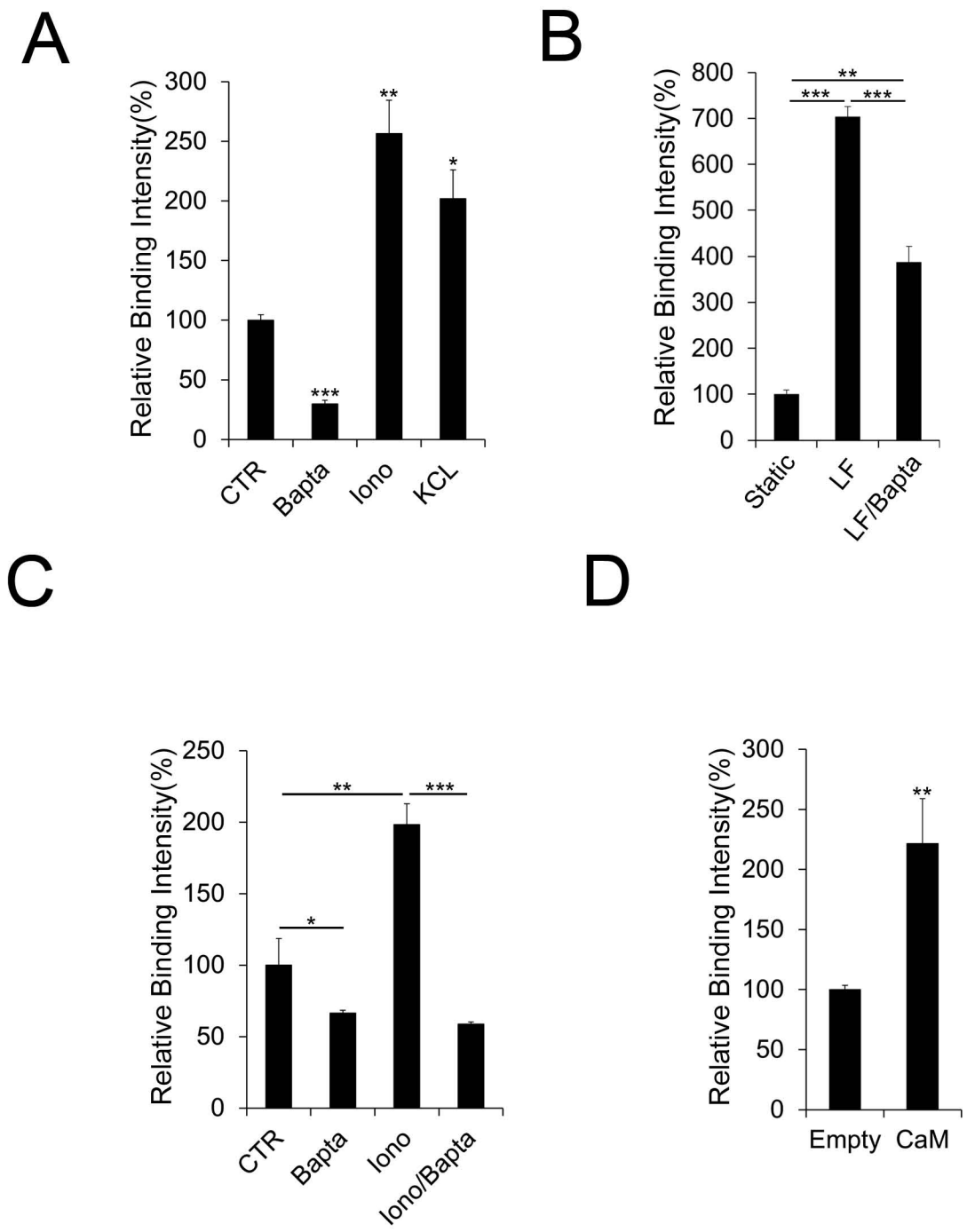

Supplemental Figure 5

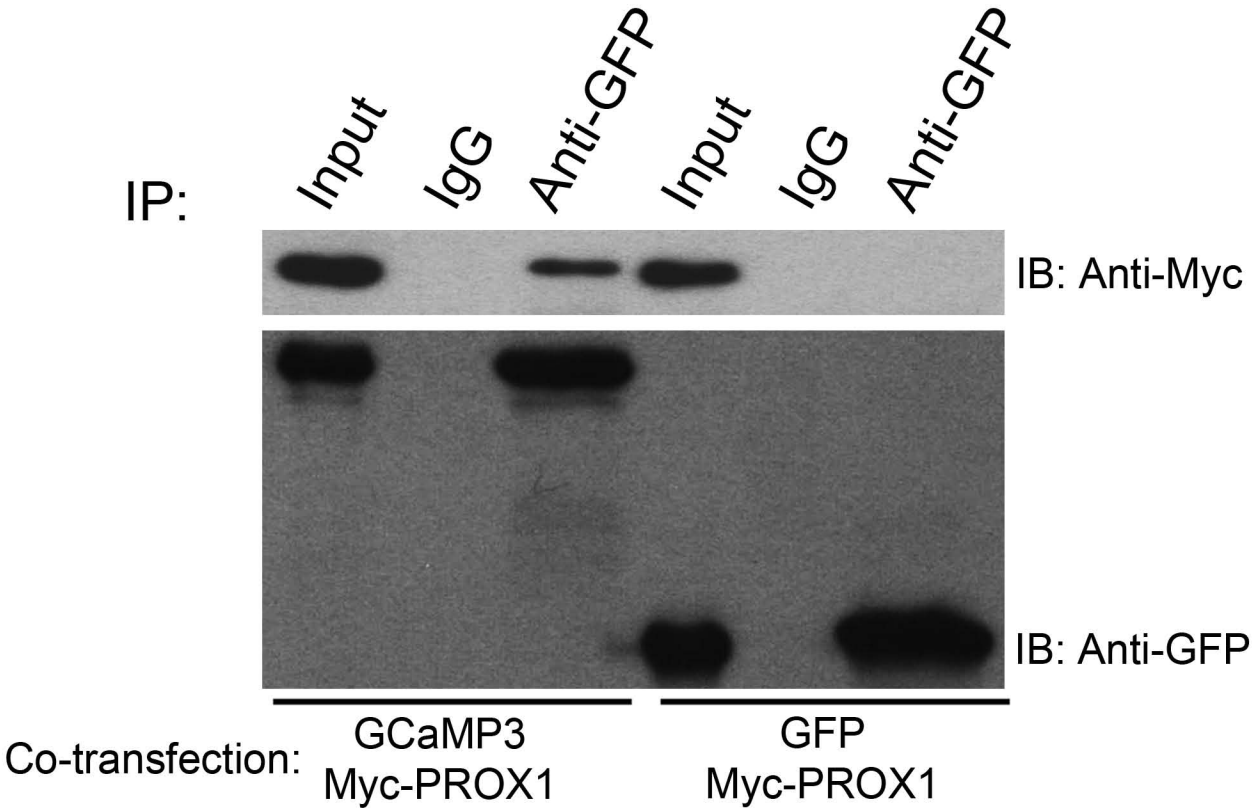

Supplemental Figure 6

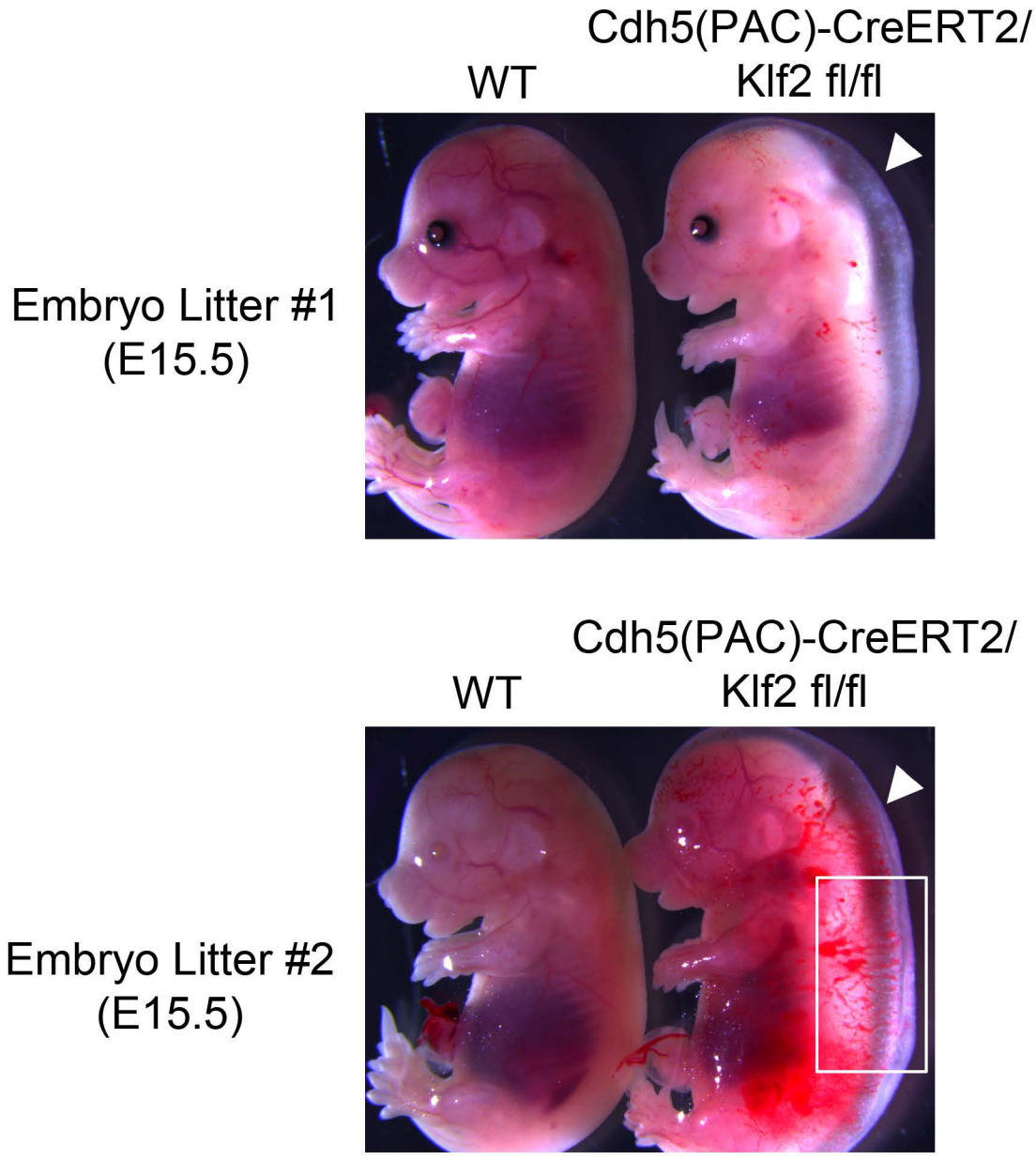

Supplemental Figure 7

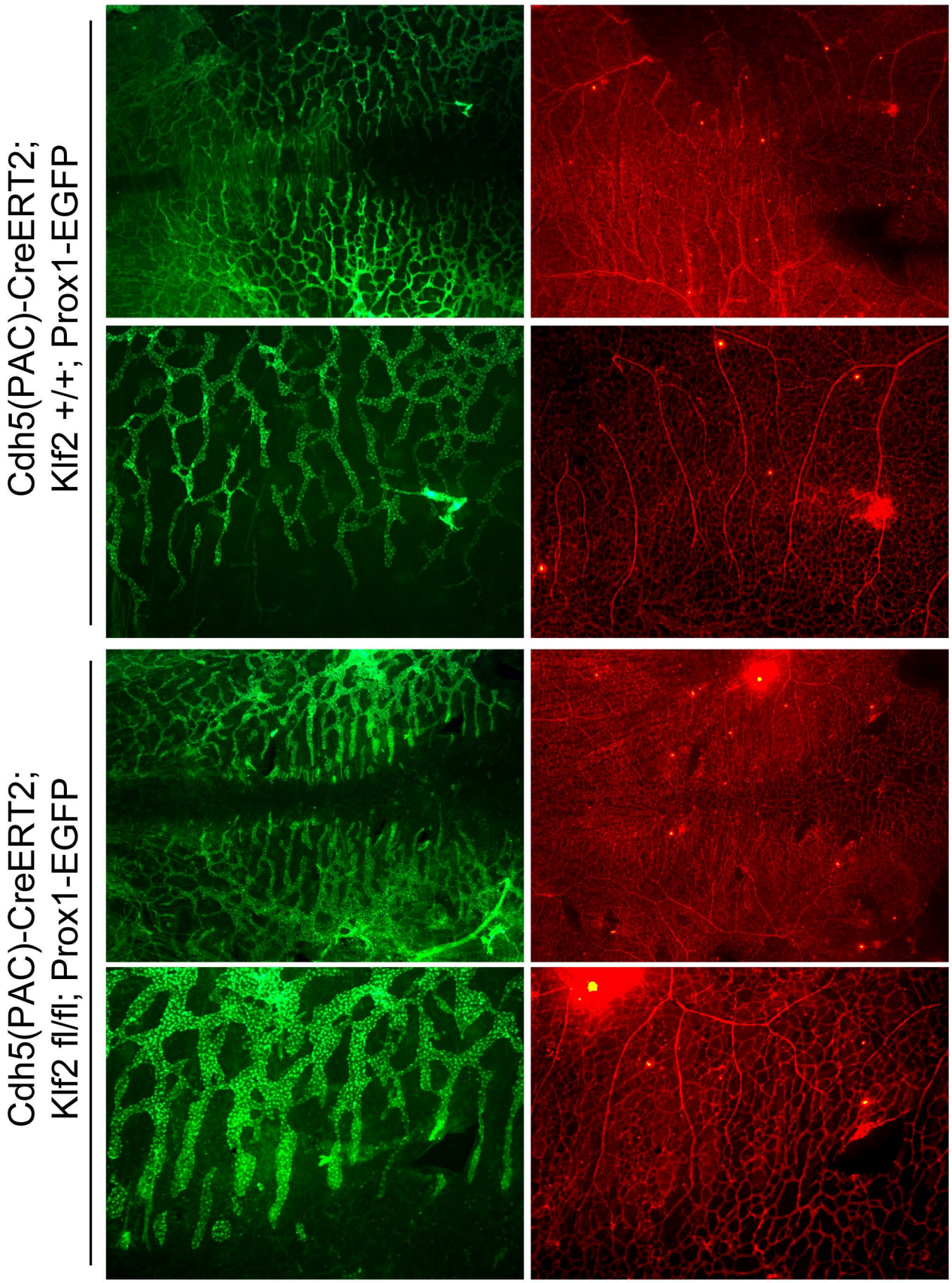

Supplemental Figure 8

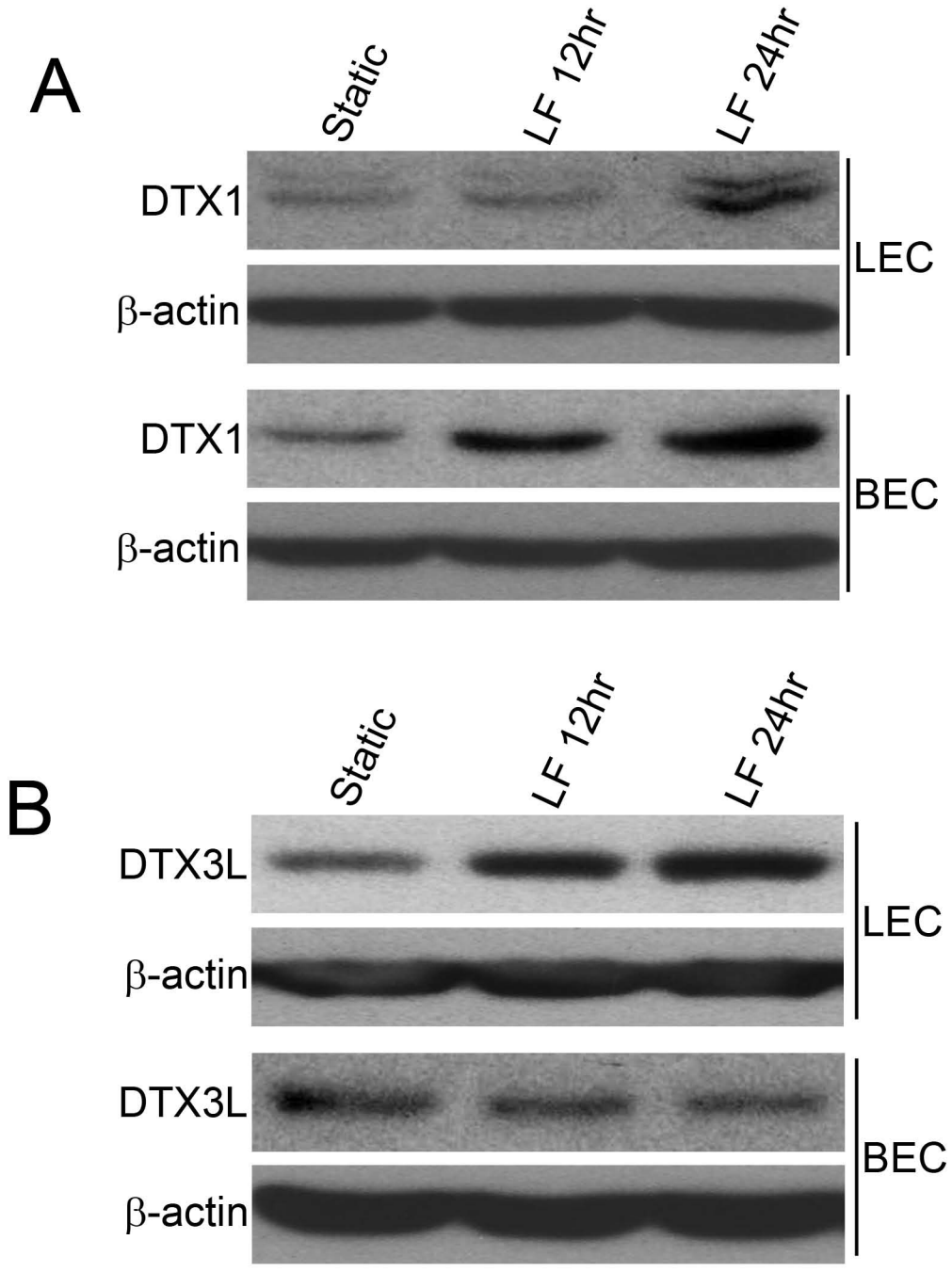

Supplemental Figure 9

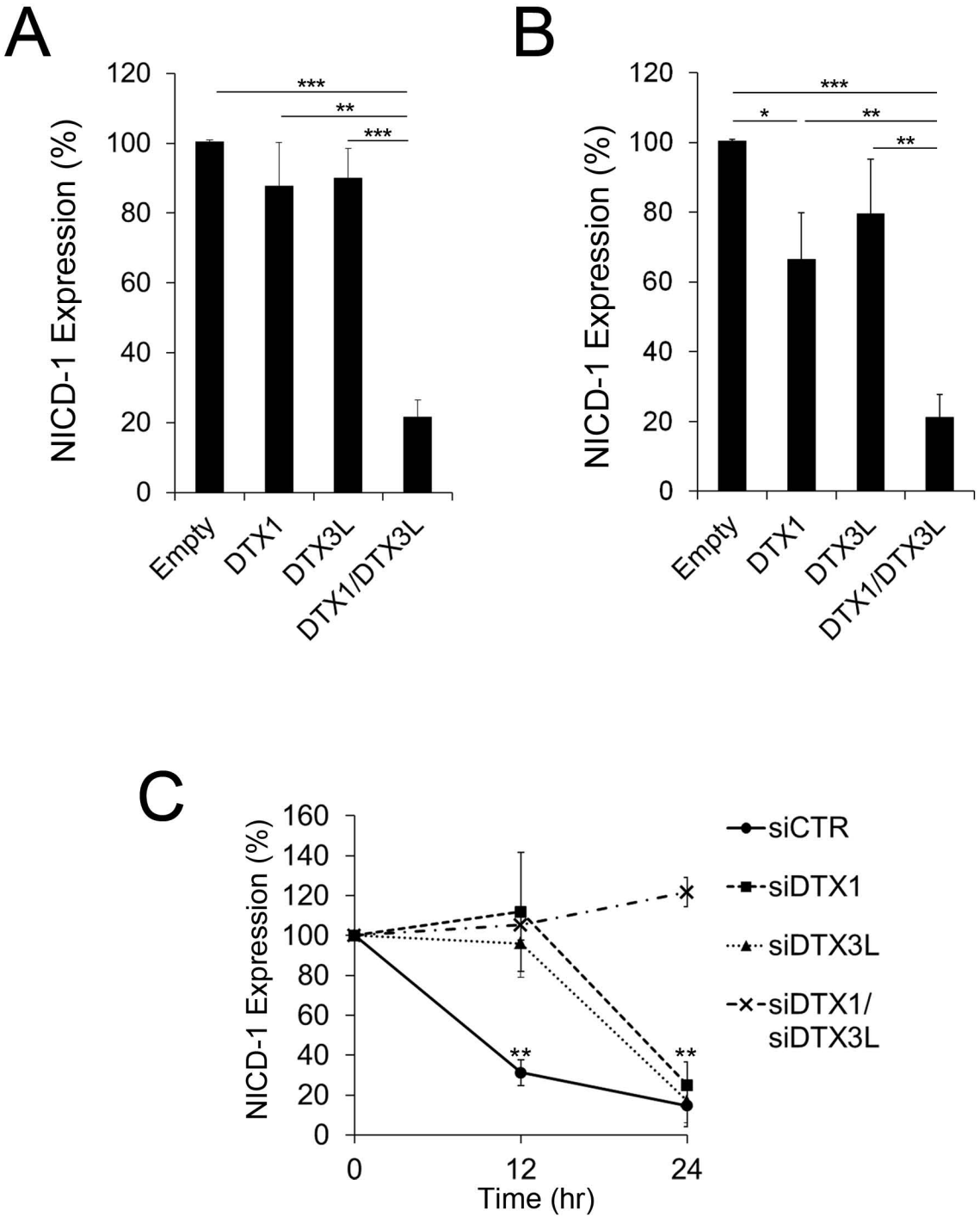

Supplemental Figure 10

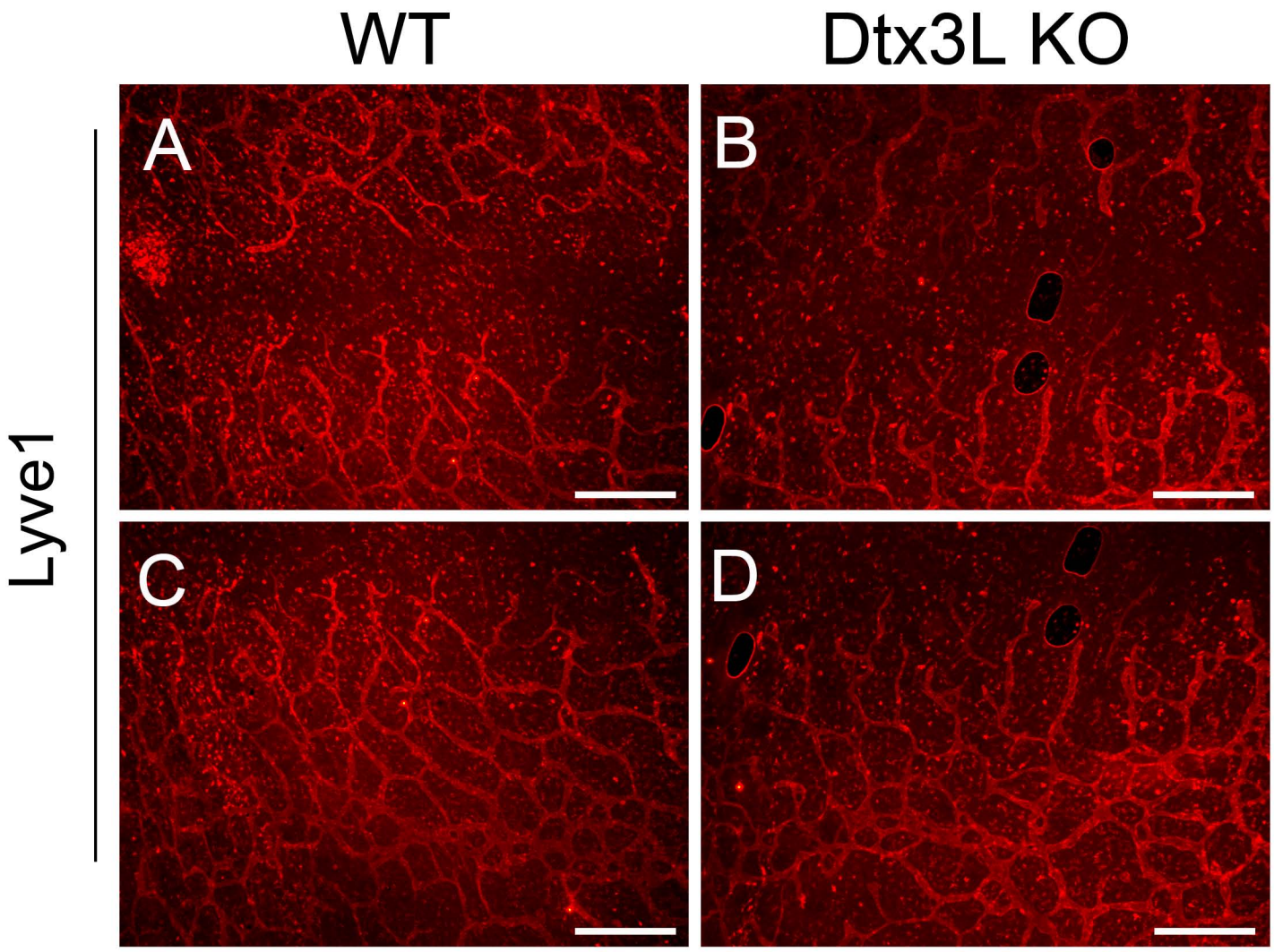

Supplemental Figure 11

Supplemental Table1. Sources of Antibodies

anti-PROX1	Rabbit polyclonal antibody was generated by the authors using a peptide (AGKDVDPSWKKAIYKV), followed by affinity purification.
anti-β-actin	Sigma-Aldrich, AC-15
anti-CD31	BD Bioscience, MEC13.3
anti-LYVE-1	Abcam, ab14917
	Angiobio, 11-034 (For mouse LEC isolation)
anti-Notch1	Santa Cruz Biotechnology, SC-6014
anti-Notch1 (cleaved at Val1744)	Cell Signaling, Cat. No. 2421
anti-Notch4	Santa Cruz Biotechnology, SC-5594
anti-Myc tag	Cell Signaling, Cat. No. 2272
	Santa Cruz Biotechnology, SC-40
anti-FLAG tag	Sigma-Aldrich, F7425, F1804
anti-HA tag	Santa Cruz Biotechnology, SC-805
	GenScript, A01244
Biotinylated goat anti-rabbit IgG	Vector Laboratories, BA-1000

Supplemental Table 2. Sequences of primers and siRNA used for this study

Human CaM fragment

Forward Primer AAA GAT ATC ATG TAC CCA TAC GAT GTT CCA GAT TAC GCT ATG GCT GAT CAG CTG ACC GAA GAA
Reverse Primer AAA CTC GAG TCA TTT TGC AGT CAT CAT CTG TAC

PROX1-D1 (YH2722)

Forward Primer AA GAA TTC ATG CCT GAC CAT GAC AGC ACA
Reverse Primer AA GTC GAC GGT GCT GGG CGG GTG TGC TGG

PROX1-D2 (YH2075)

Forward Primer AA GAA TTC ATG AAC AAA AAT GGT GGC ACG
Reverse Primer AA GTC GAC GGG ACT CAC AGA CTG CGG GGC

PROX1-D3 (YH2076)

Forward Primer AA GAA TTC CGA GAA AGT TAC AGA GAA AAC
Reverse Primer AA GTC GAC GCA CAT CTC ATT ATC TGA CCT

PROX1-D4 (YH2077)

Forward Primer AA GAA TTC GAG CTA GAC CCA GGA CAG TTT
Reverse Primer AA GTC GAC GTG GTT TTC CCC ATT GAC TGC

PROX1-D5 (YH2078)

Forward Primer AA GAA TTC AAT TTC CAC ACC GCC AAC CAG
Reverse Primer AA GTC GAC GGG AGC ACC TAA TGG GCT CTG

PROX1-D6 (YH2079)

Forward Primer AA GAA TTC TCC GGC TCC TTC TCT GGA AAA
Reverse Primer AA GTC GAC GGA GCT GGG ATA ACG GGT ATA

PROX1-D7 (YH2080)

Forward Primer AA GAA TTC AAT ATG CTG AAG ACC TAC TTC
Reverse Primer AA GTC GAC CTA CTC ATG AAG CAG CTC TTG

Mouse Dtx3L

Forward Primer TTC ACC ATG GAC TAC AAA GAC GAT GAC GAC AAG GCT TCC AGT CCC GAC CCG CCG
Reverse Primer TAT GCG GCC GCT TAC TCA ATG CCT TTT GCT TTCA

Dtx3L-transgenic vector (YH3004)

Forward Primer GGC GTG TAC GGT GGG AGG

Reverse Primer GCT TTA ATT AAG GTT CTT TCC GCC TCA GAAG

PROX1 V19D Mutagenesis

Forward Primer CAA ACC AAG AGG AGA AGA GAT GAC ATT GGA GTG

Reverse Primer CCC TAC CGT CCT TTT CAC TCC AAT GTC ATC TCT

PROX1 I21D Mutagenesis

Forward Primer AAG AGG AGA AGA GTT GAC GAT GGA GTG AAA AGG

Reverse Primer TGC TGT CCC TAC CGT CCT TTT CAC TCC ATC GTC

PROX1 V23D Mutagenesis

Forward Primer AGA AGA GTT GAC ATT GGA GAT AAA AGG ACG GTA

Reverse Primer TGC AGA TGC TGT CCC TAC CGT CCT TTT ATC TCC

PROX1 V27D Mutagenesis

Forward Primer ATT GGA GTG AAA AGG ACG GAT GGG ACA GCA TCT

Reverse Primer CTT AGC AAA AAA TGC AGA TGC TGT CCC ATC CGT

PROX1 A30D Mutagenesis

Forward Primer AAA AGG ACG GTA GGG ACA GAT TCT GCA TTT TTT

Reverse Primer TGC TCT TGC CTT AGC AAA AAA TGC AGA ATC TGT

PROX1 A32D Mutagenesis

Forward Primer ACG GTA GGG ACA GCA TCT GAT TTT TTT GCT AAG

Reverse Primer AAA CGT TGC TCT TGC CTT AGC AAA AAA ATC AGA

PROX1 A33D Mutagenesis

Forward Primer GTA GGG ACA GCA TCT GCA GAT TTT GCT AAG GCA

Reverse Primer AAA AAA CGT TGC TCT TGC CTT AGC AAA ATC TGC

PROX1 A34D Mutagenesis

Forward Primer GGG ACA GCA TCT GCA TTT GAT GCT AAG GCA AGA

Reverse Primer ACT AAA AAA CGT TGC TCT TGC CTT AGC GAT AAA

siRNA for human ORAI1

UCACUGGUUAGCCAUAAGA

siRNA for human KLF2

CCAAGAGUUCGCAUCUGAAdTdT

siRNA for human DTX1

CCAAGAAGAAGCACCUUAAdTdT

siRNA for human DTX3L

GCCAAGACAUUGGAGAAGUdTdT

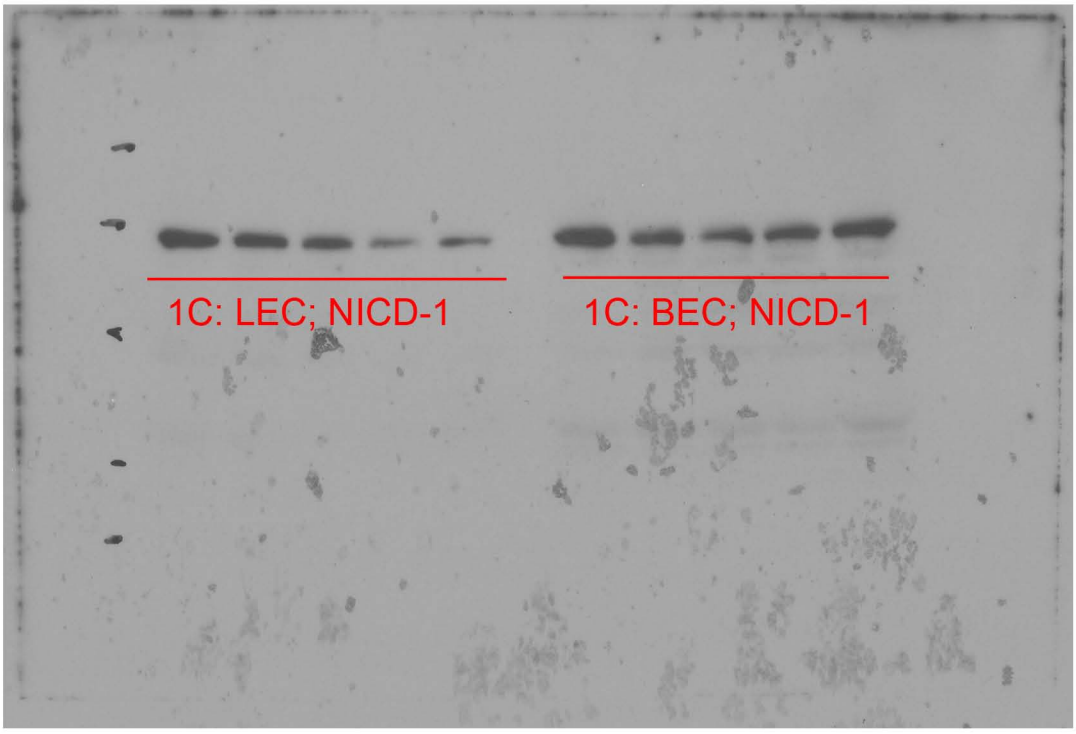

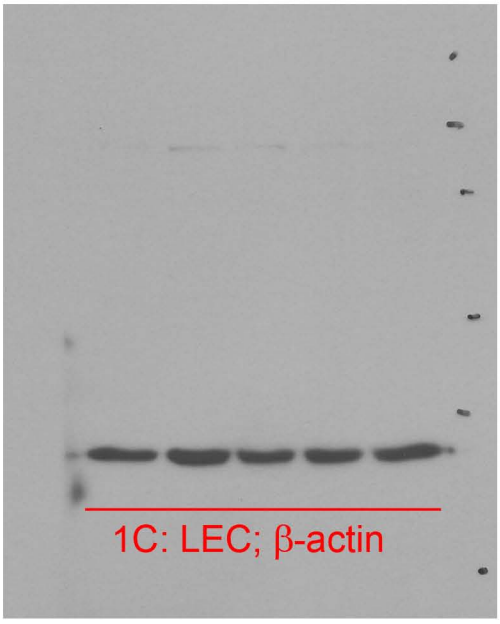

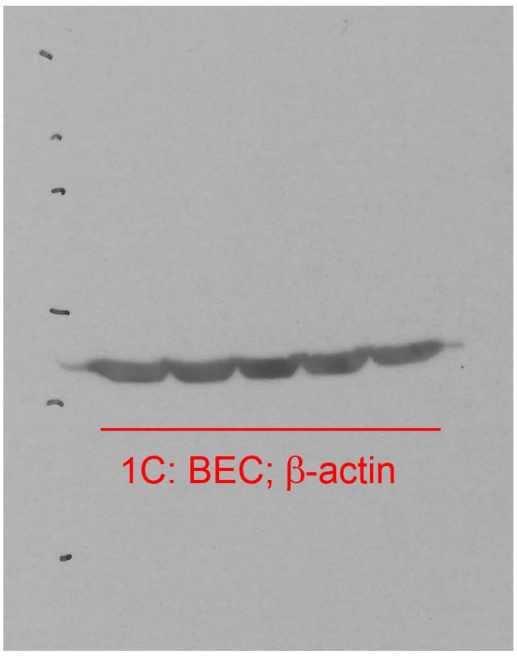

Full unedited gel for Figure 1C

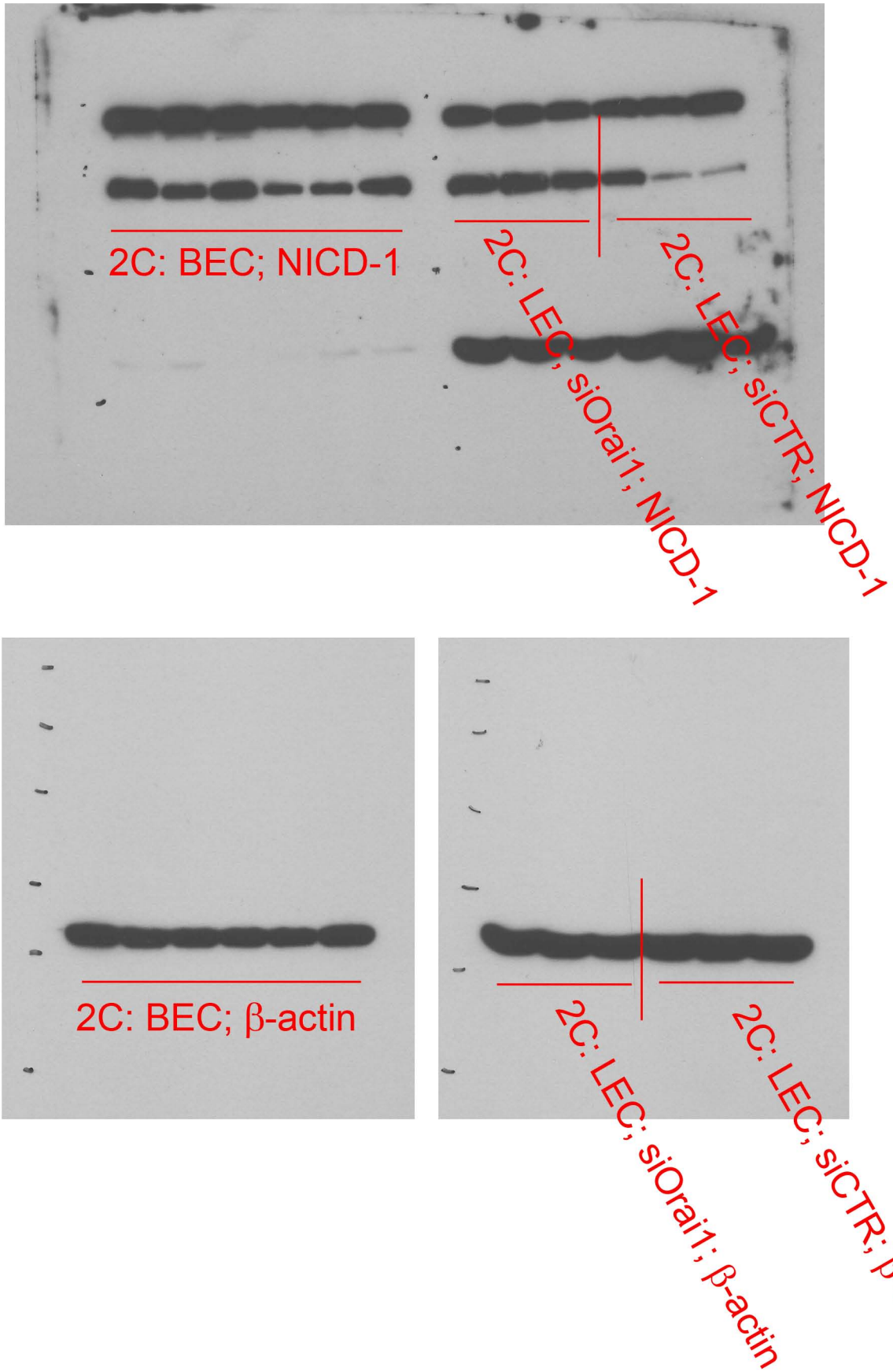

Full unedited gel for Figure 2C

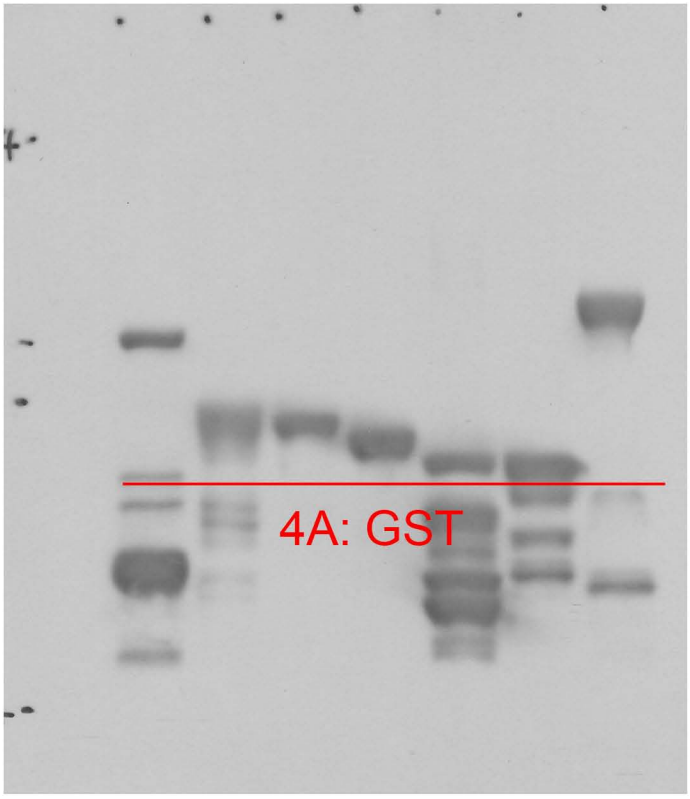

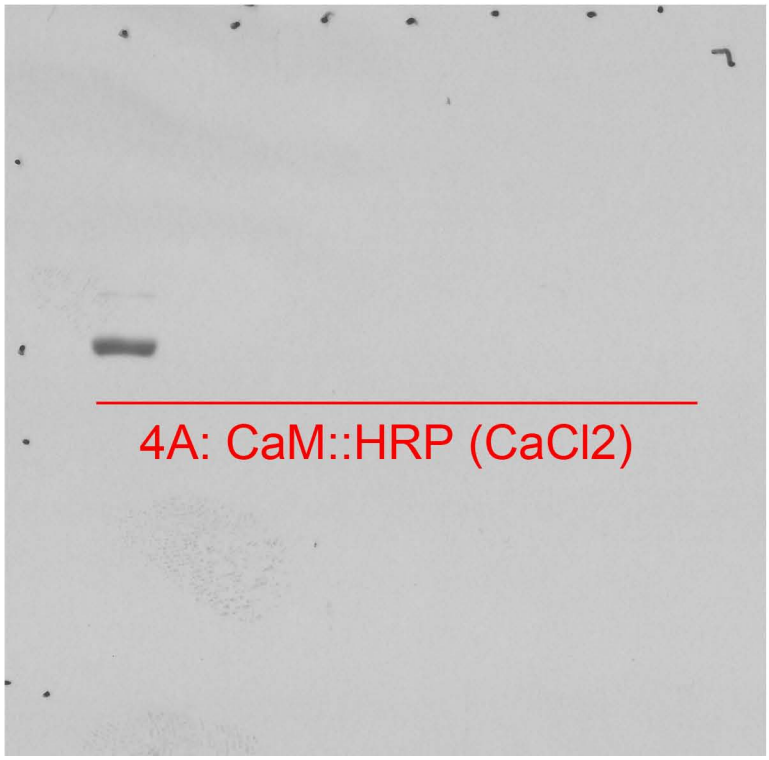

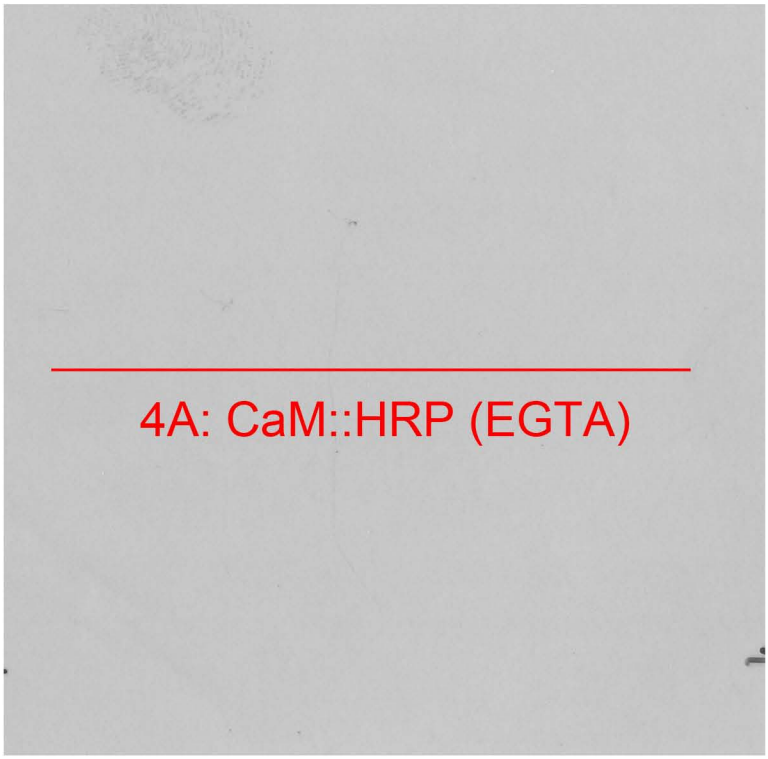

Full unedited gel for Figure 4A

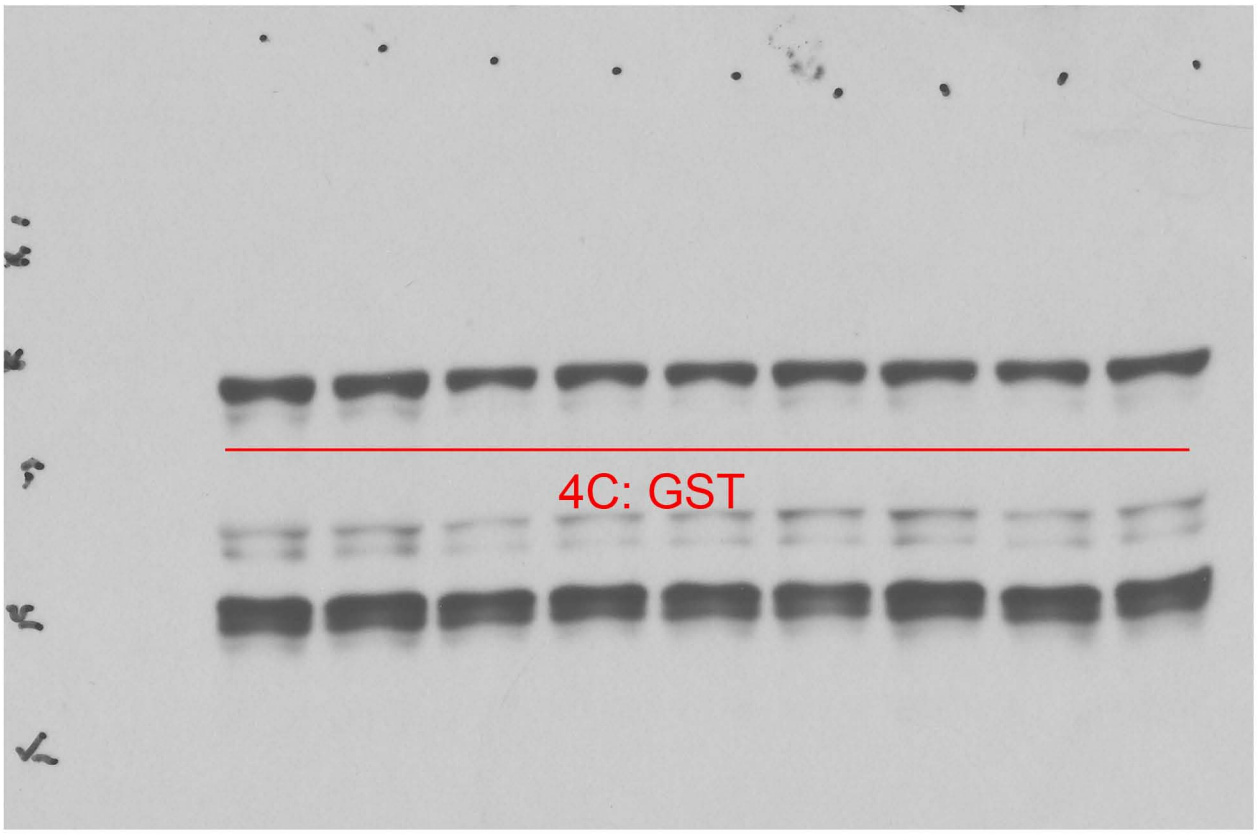

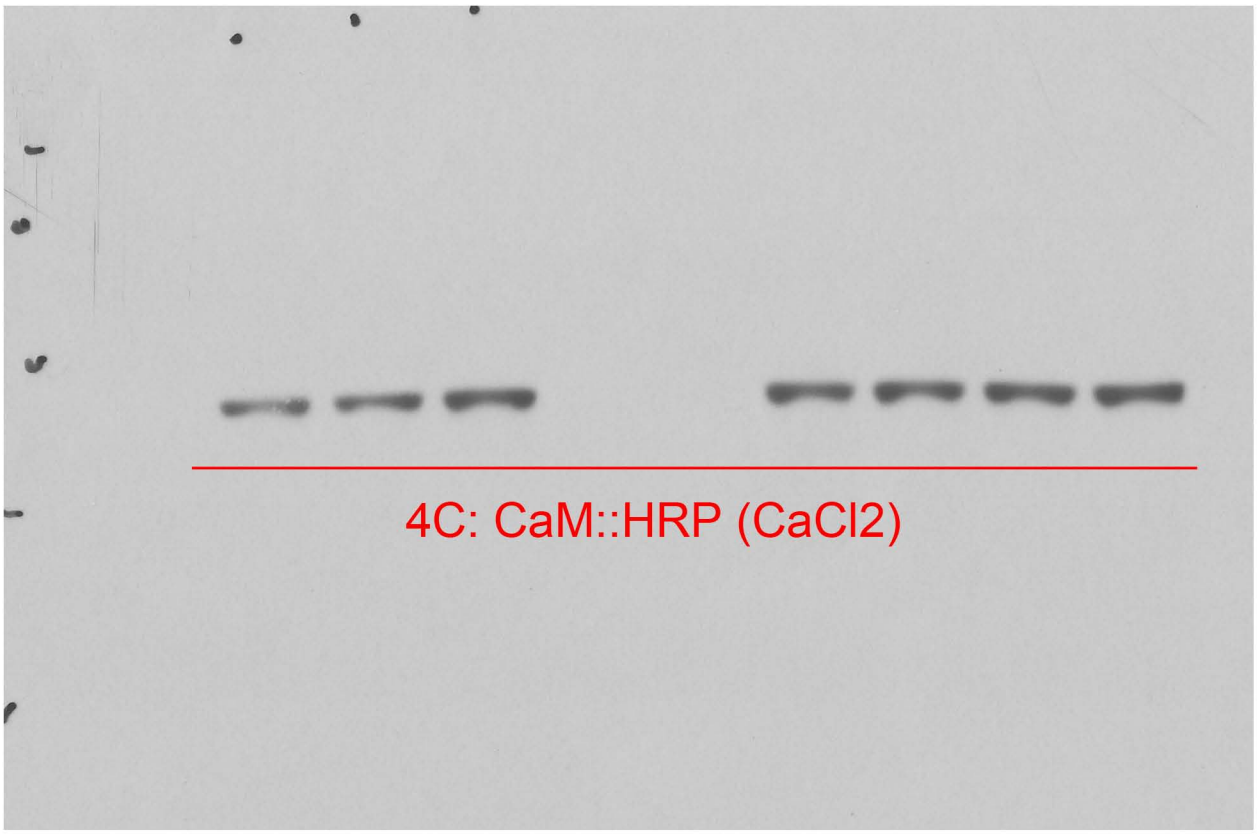

Full unedited gel for Figure 4C

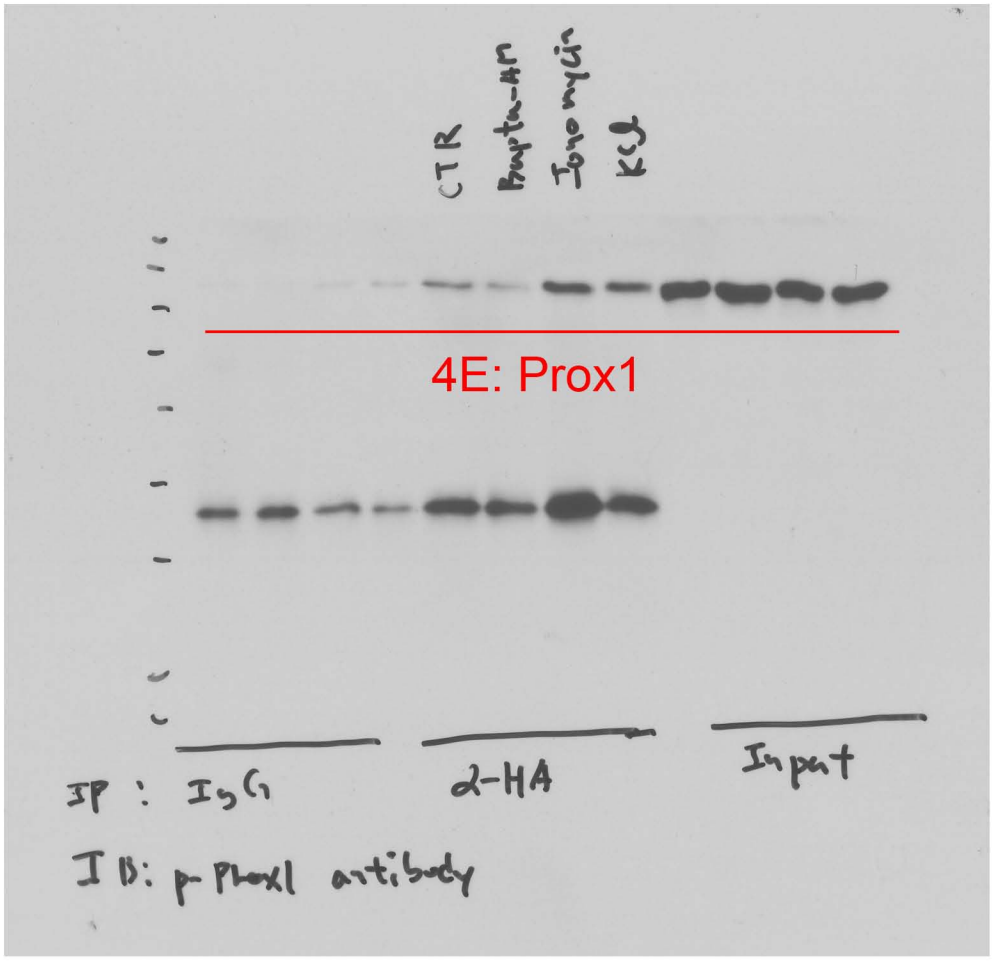

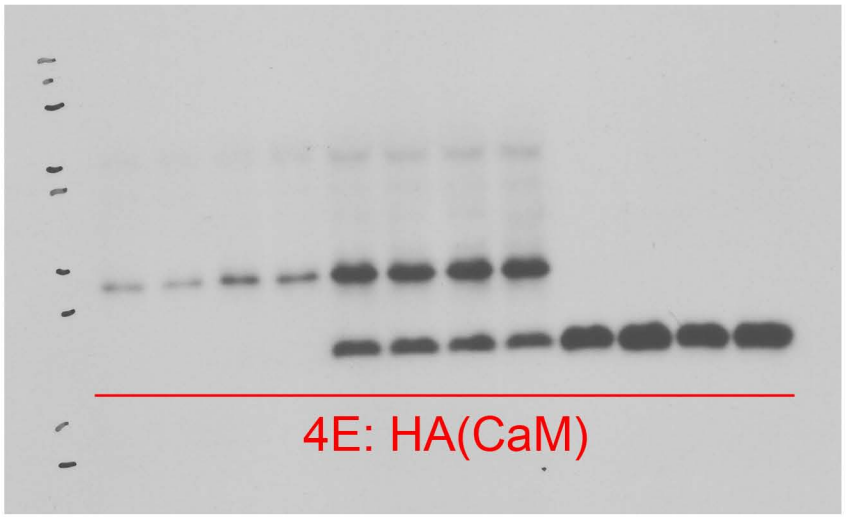

Full unedited gel for Figure 4E

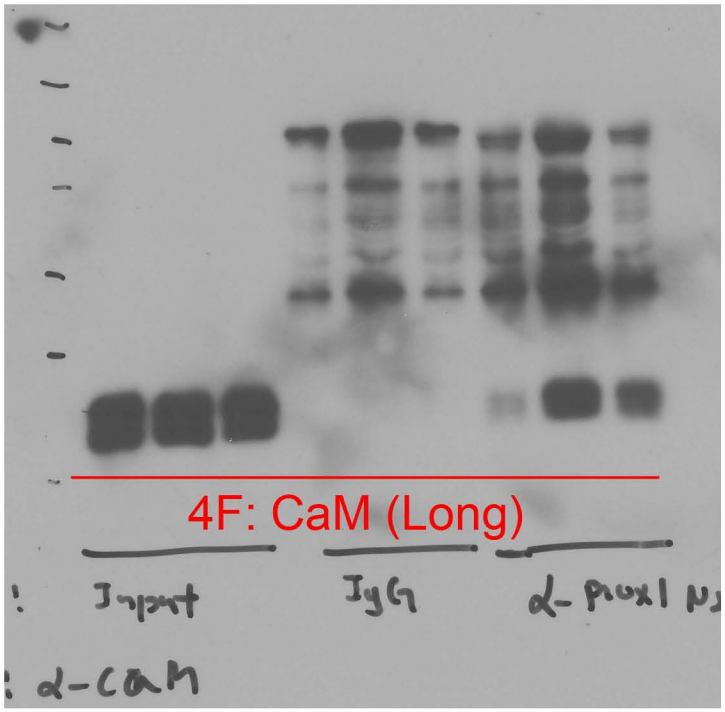

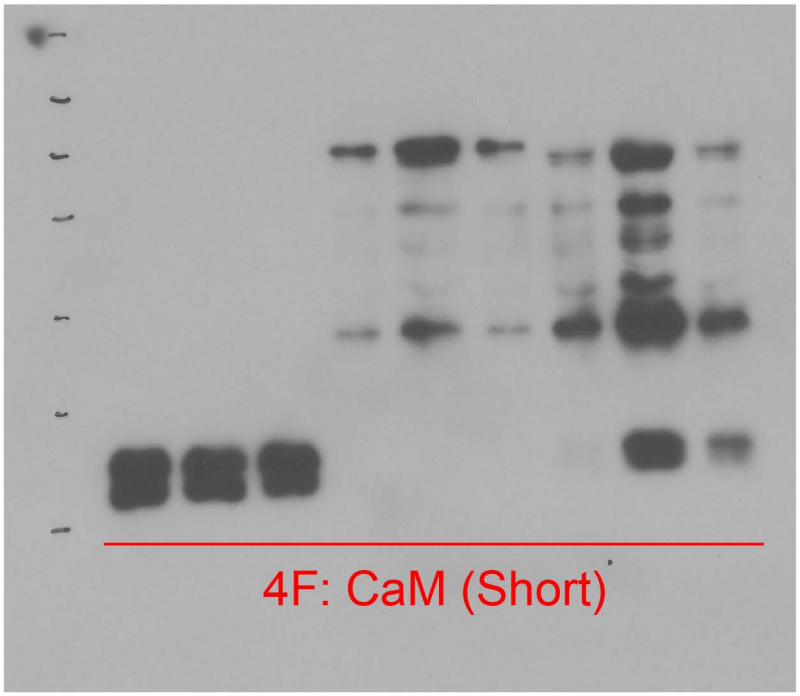

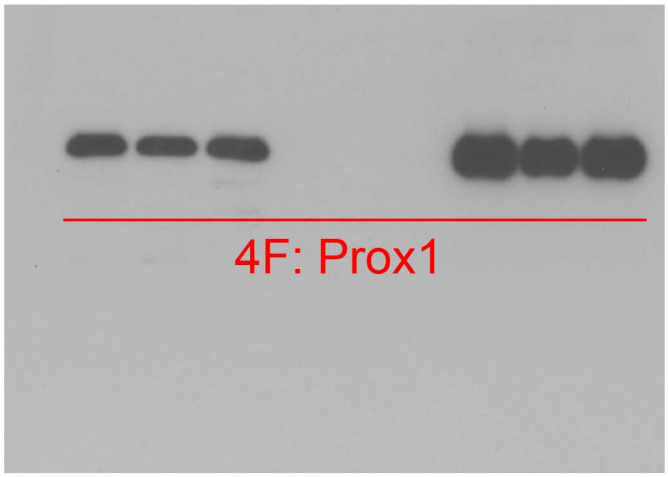

Full unedited gel for Figure 4F

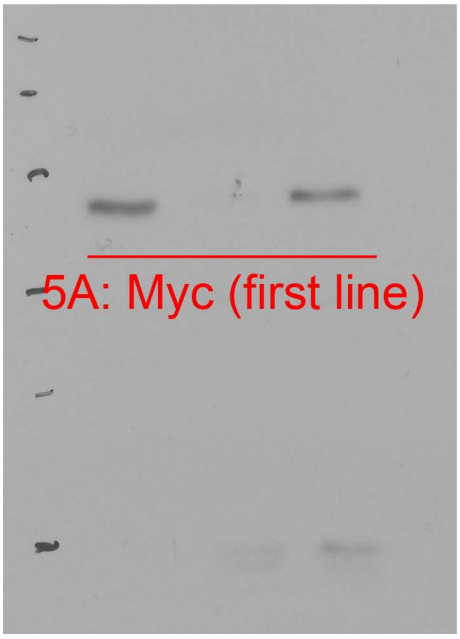

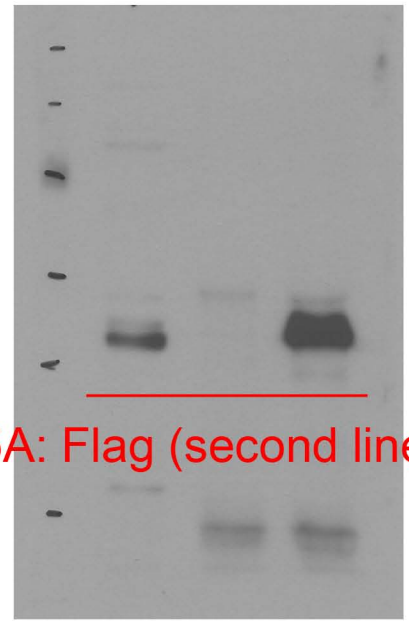

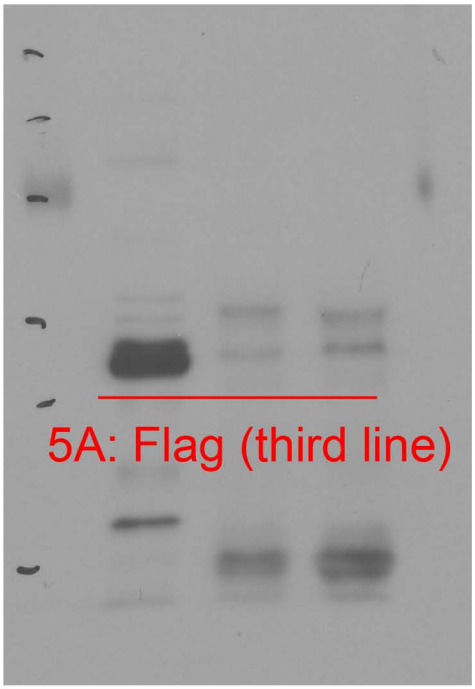

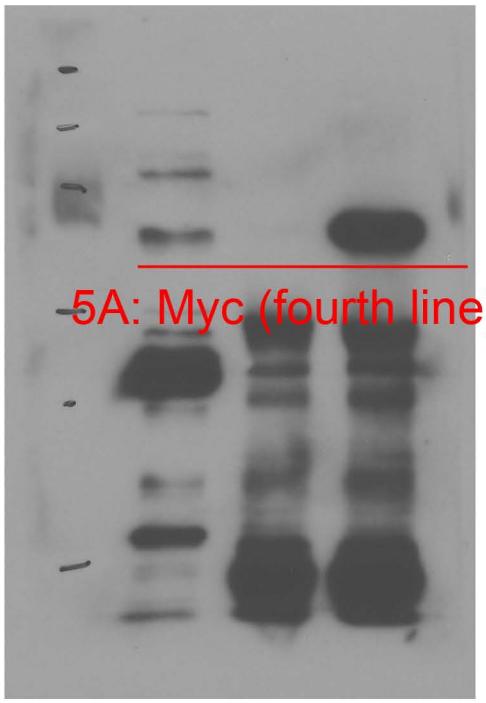

Full unedited gel for Figure 5A

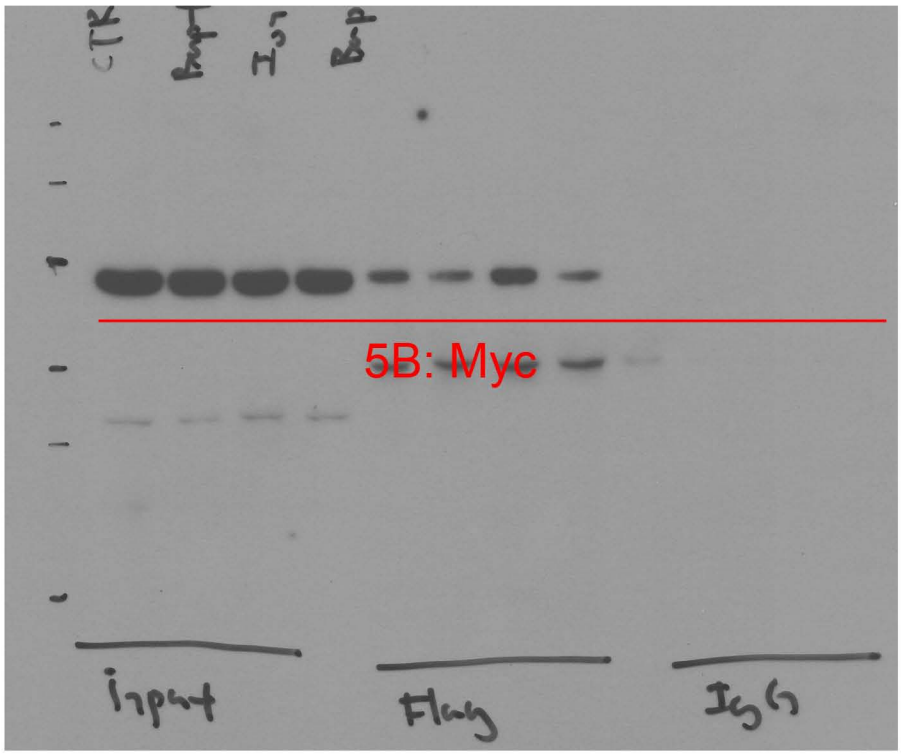

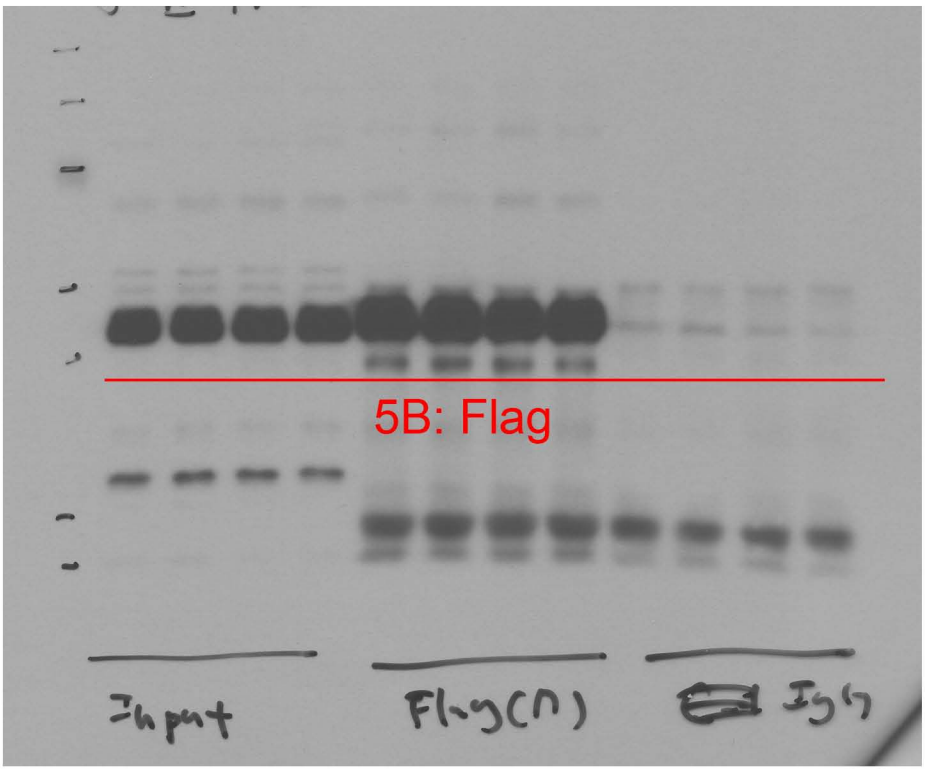

Full unedited gel for Figure 5B

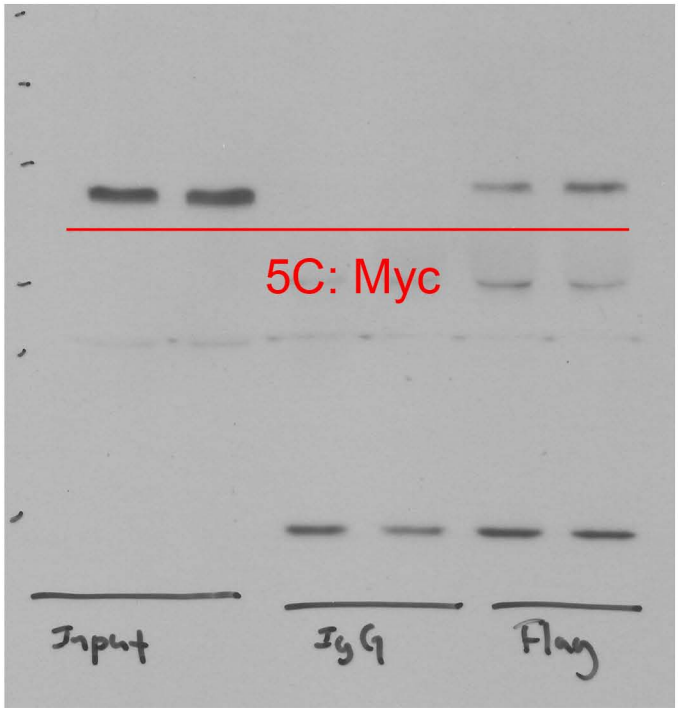

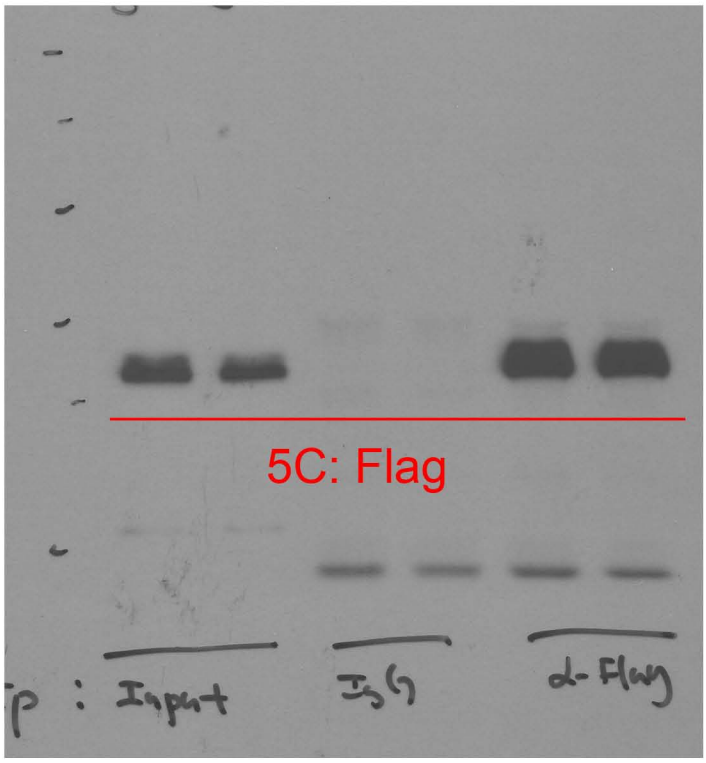

Full unedited gel for Figure 5C

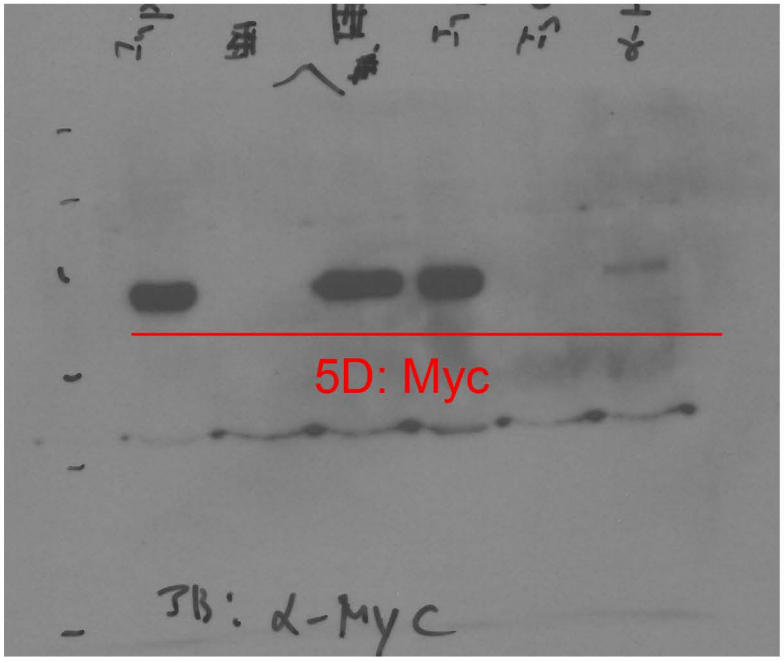

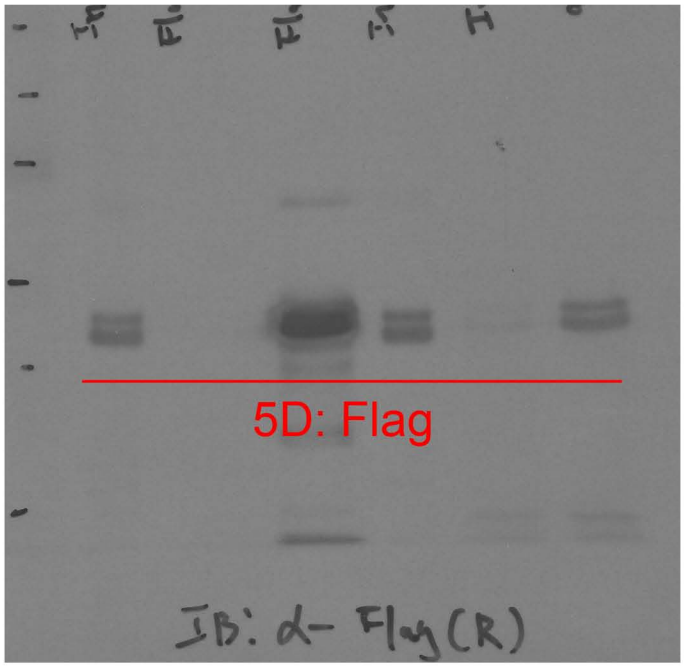

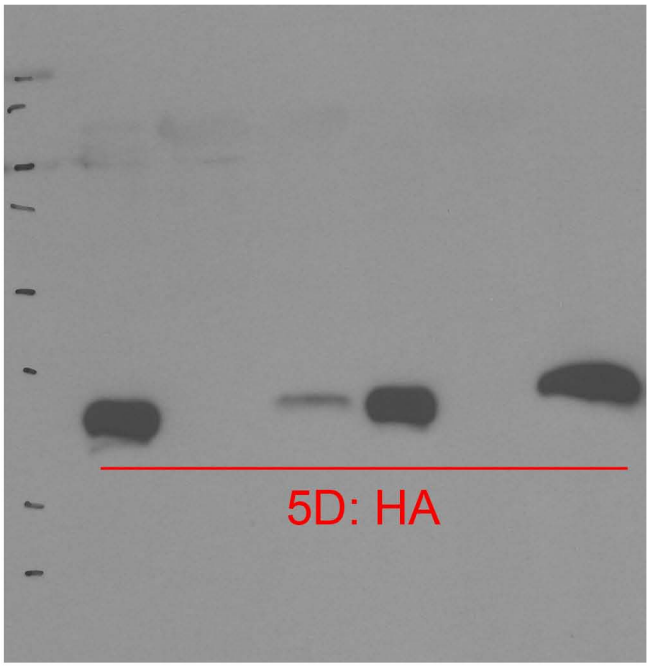

Full unedited gel for Figure 5D

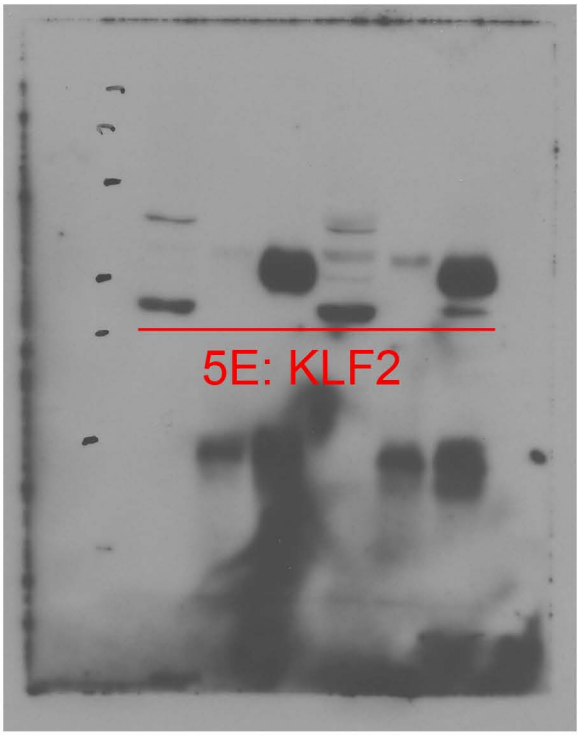

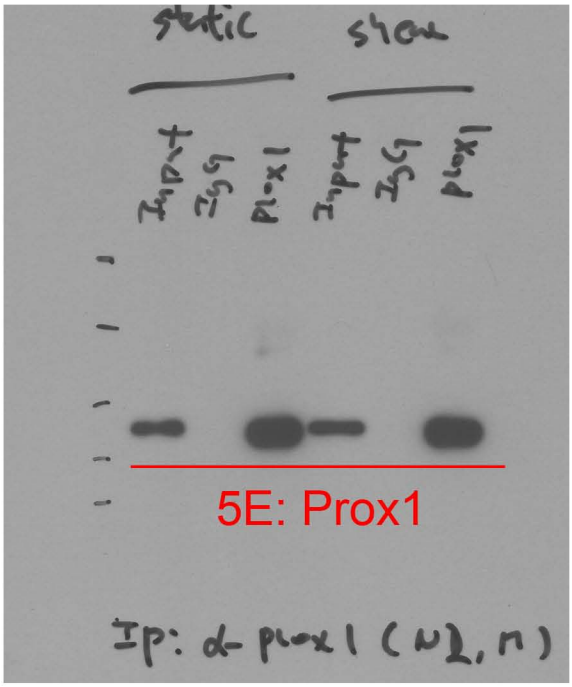

Full unedited gel for Figure 5E

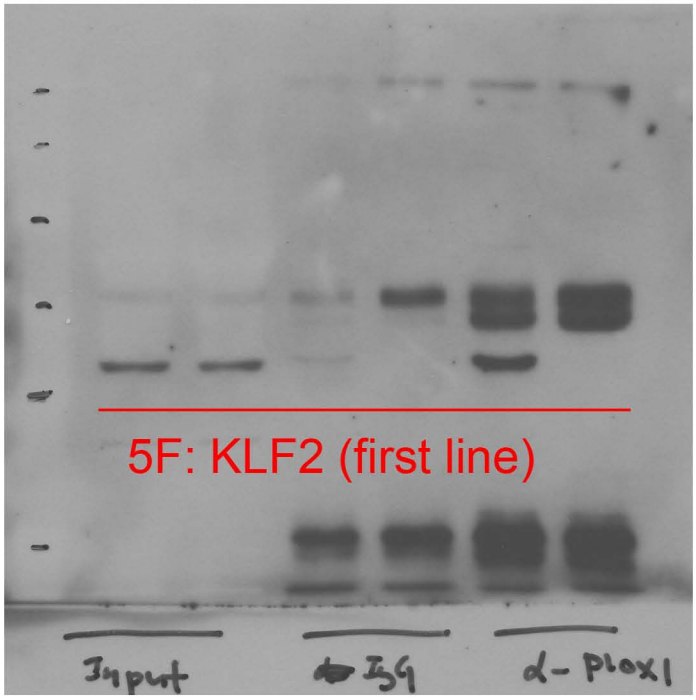

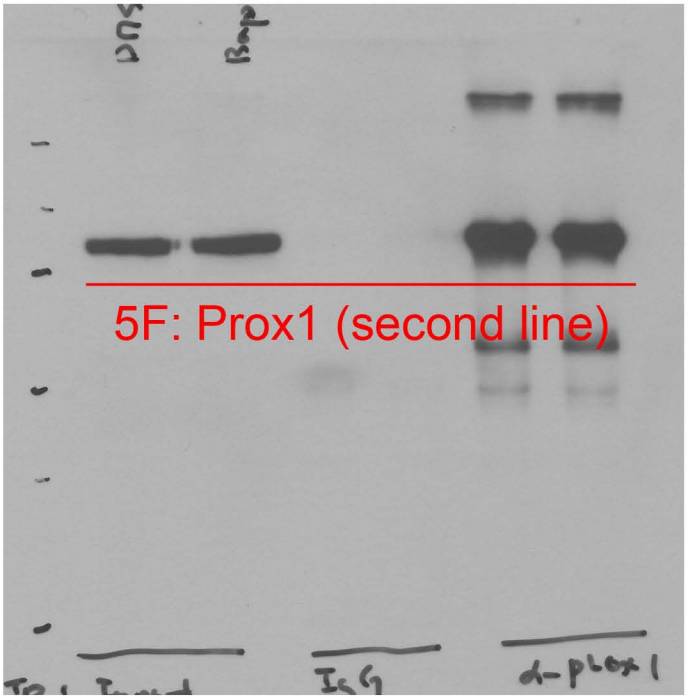

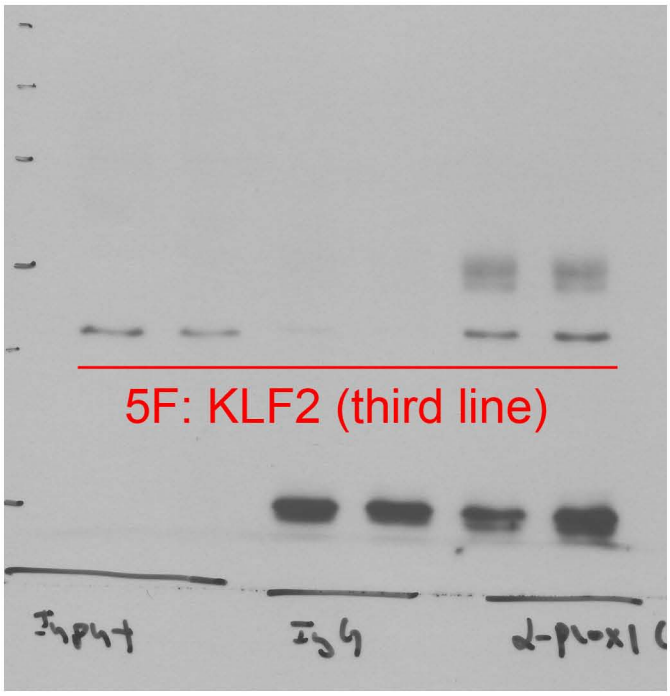

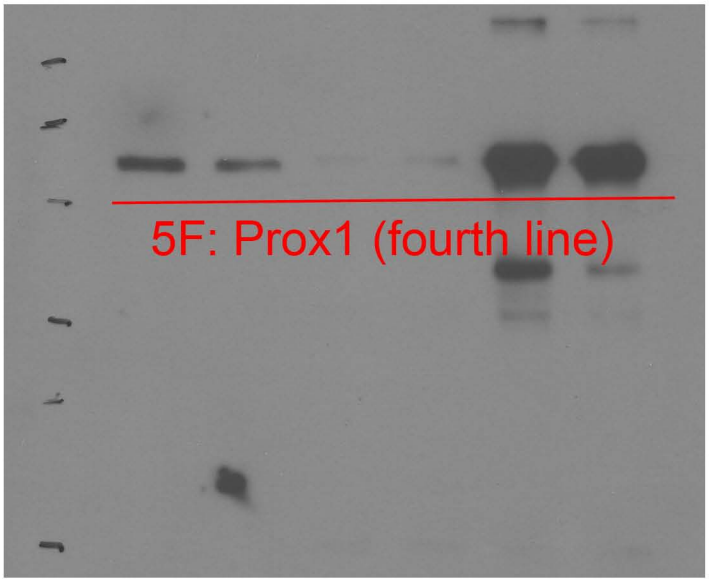

Full unedited gel for Figure 5F

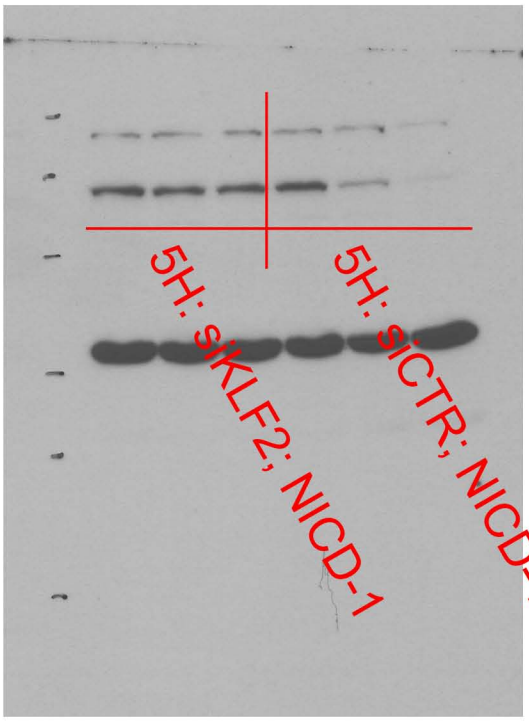

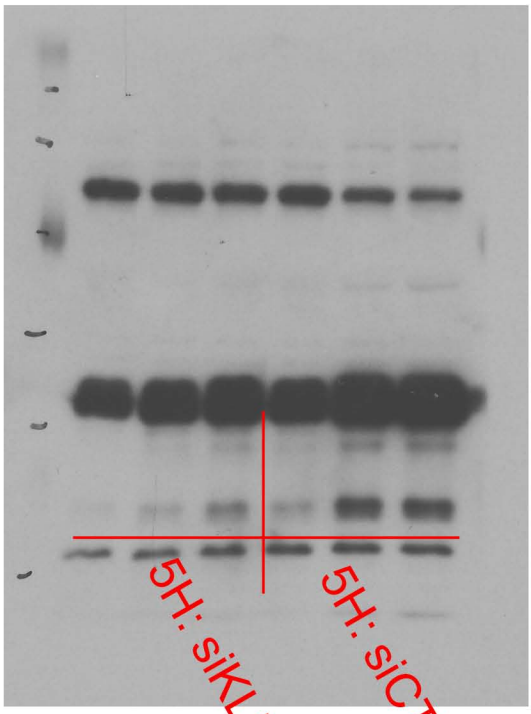

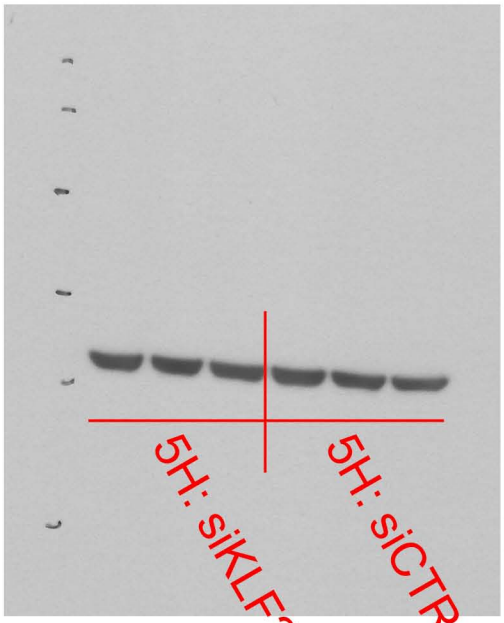

Full unedited gel for Figure 5H

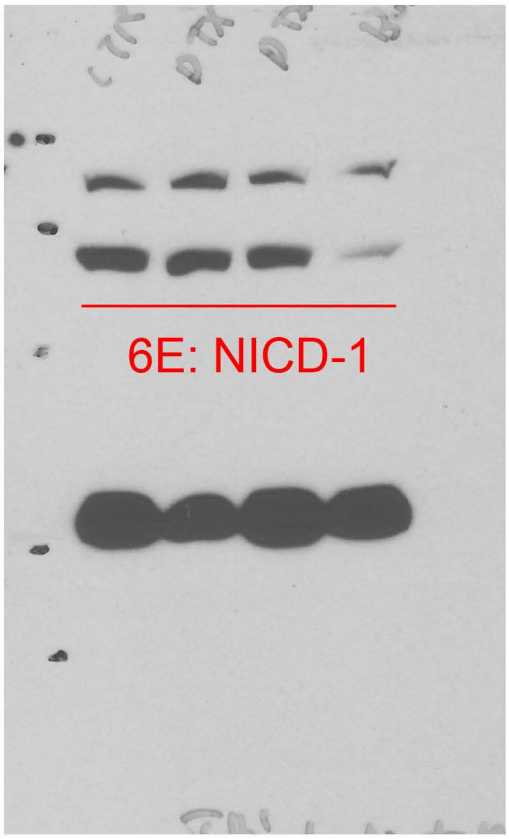

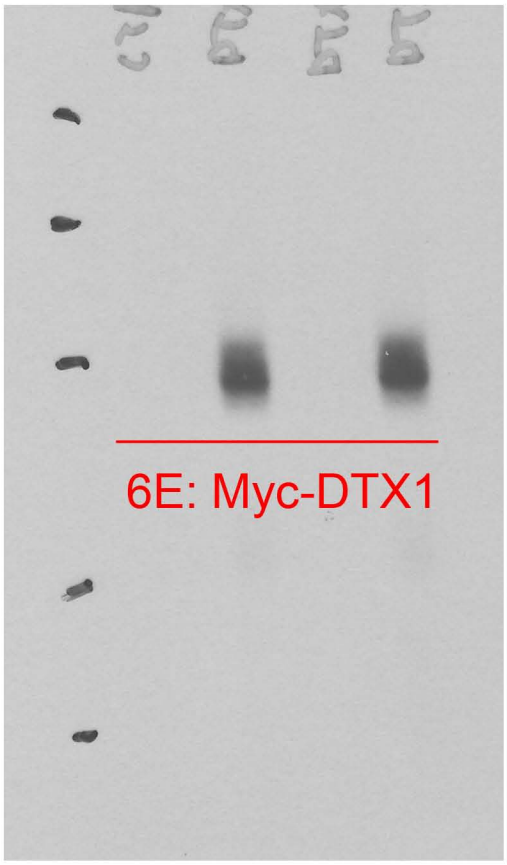

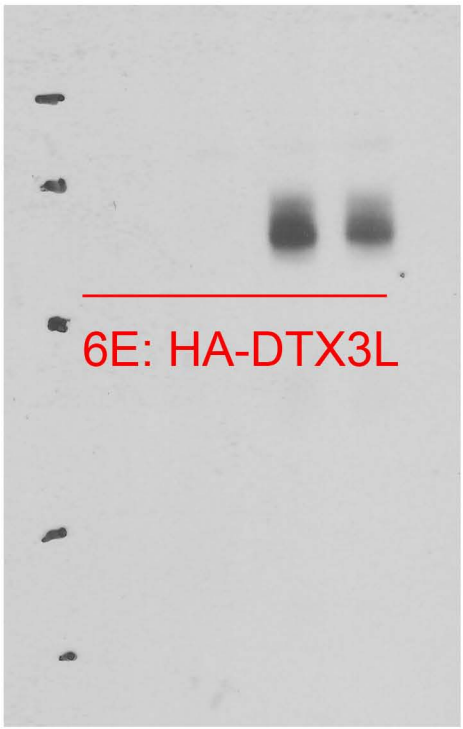

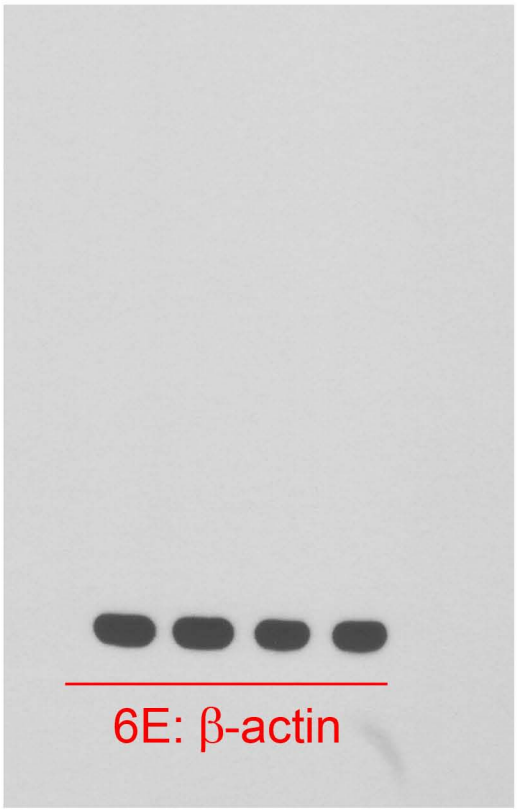

Full unedited gel for Figure 6E

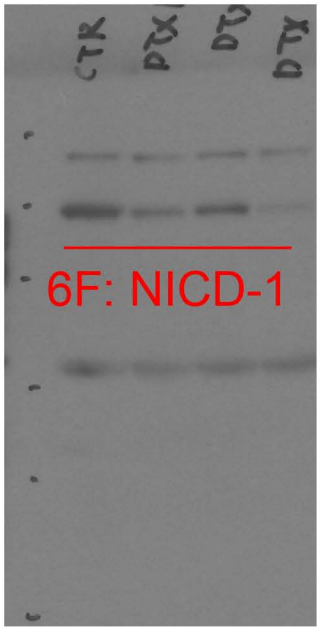

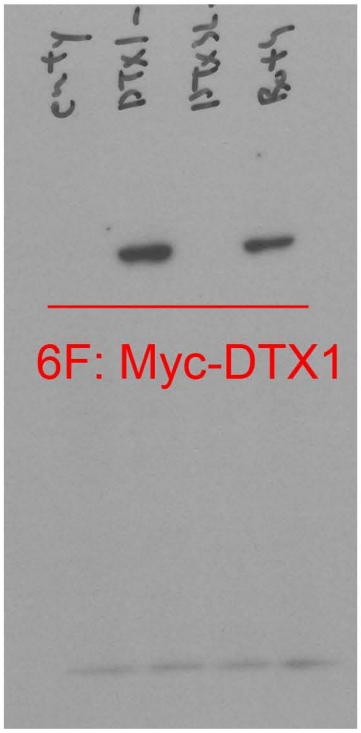

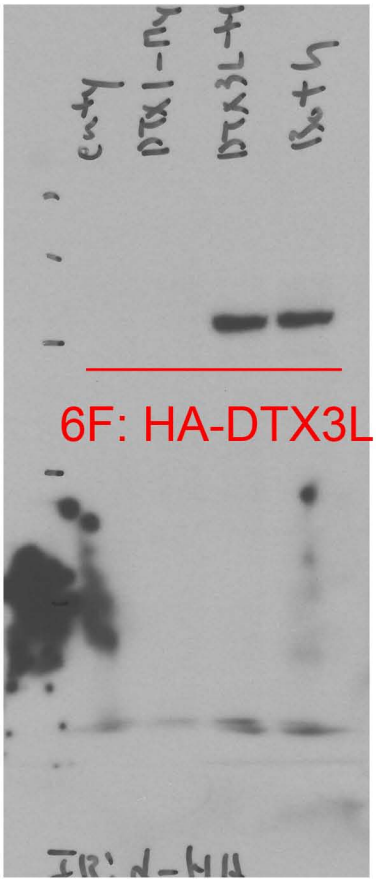

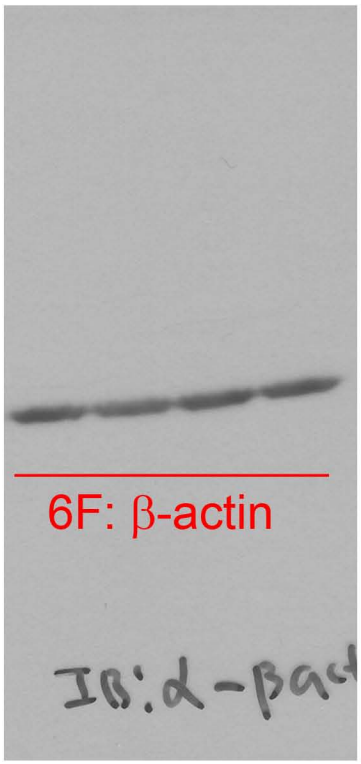

Full unedited gel for Figure 6F

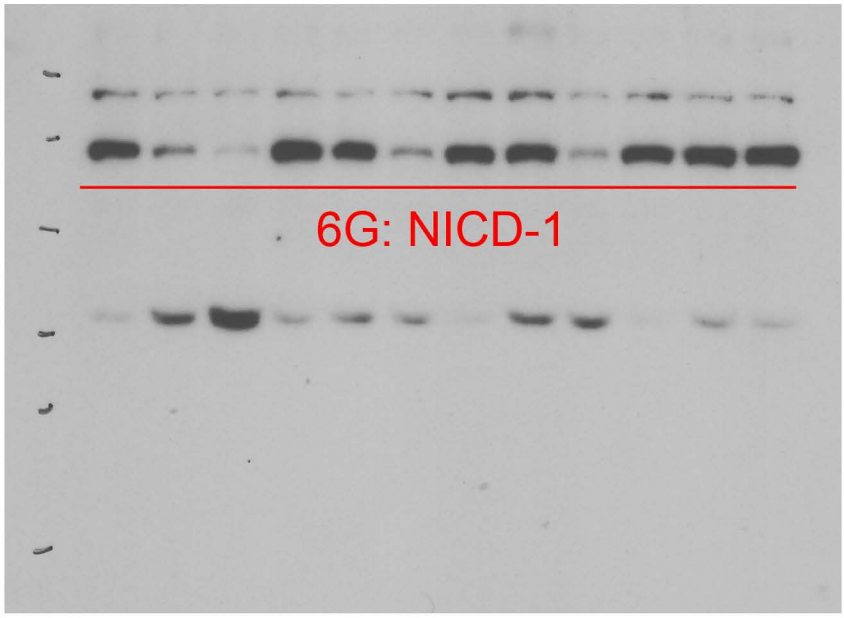

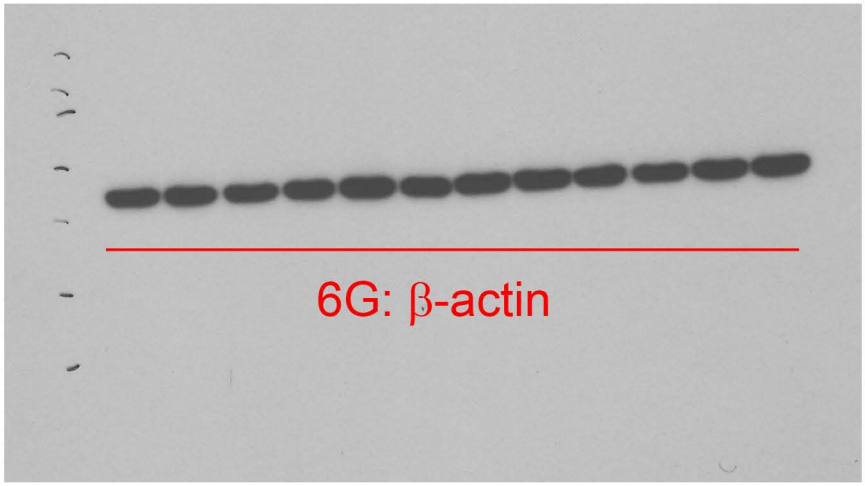

Full unedited gel for Figure 6G

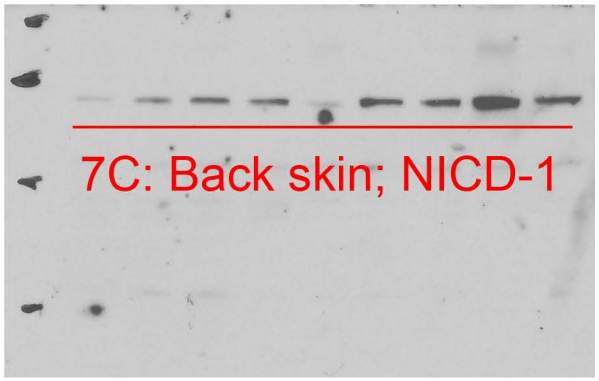

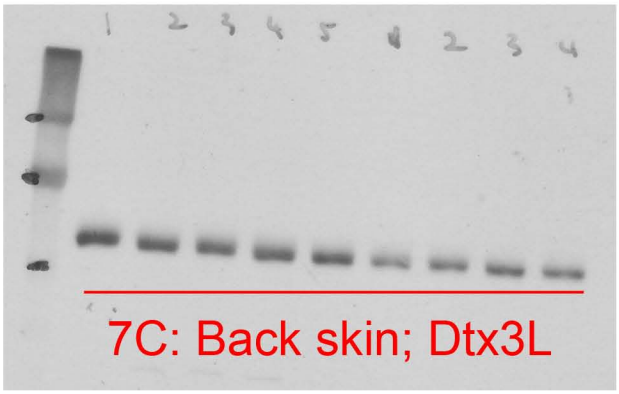

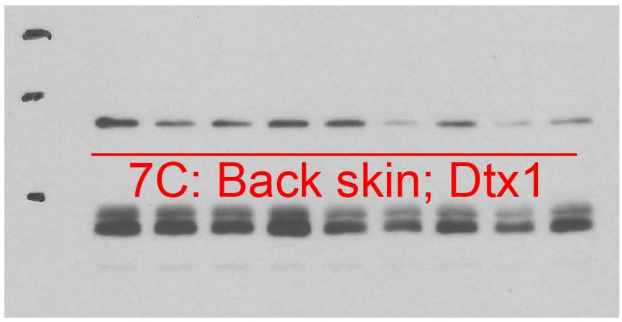

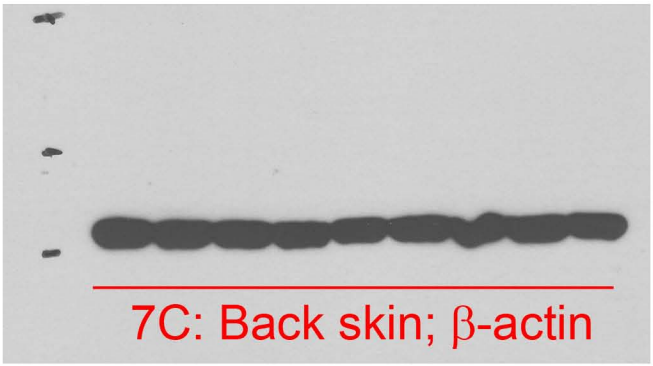

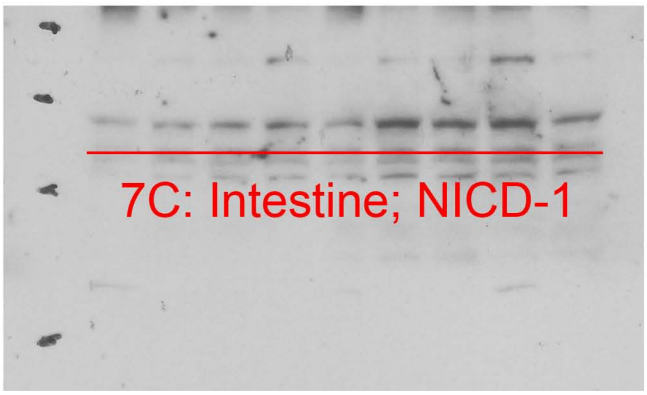

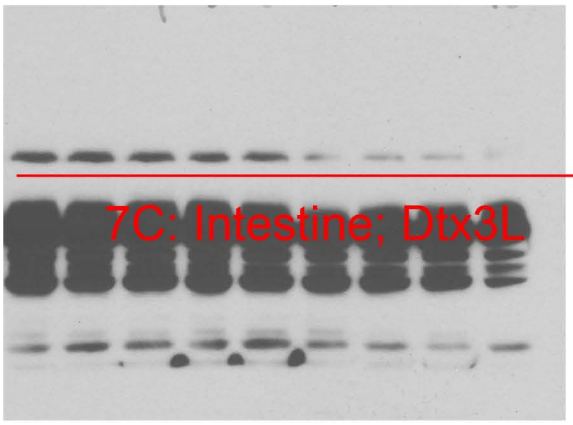

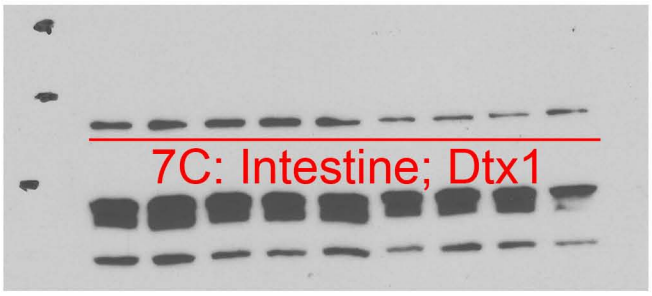

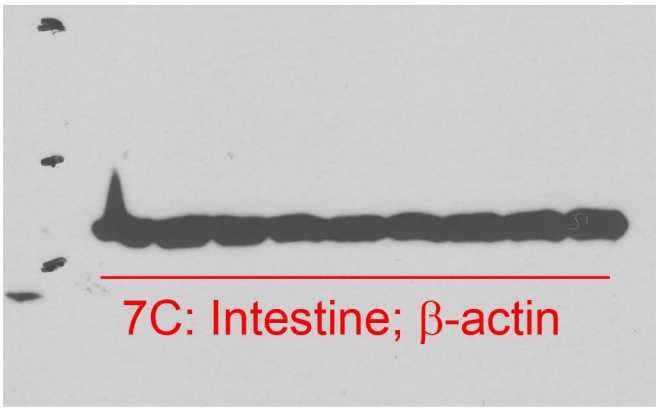

Full unedited gel for Figure 7C

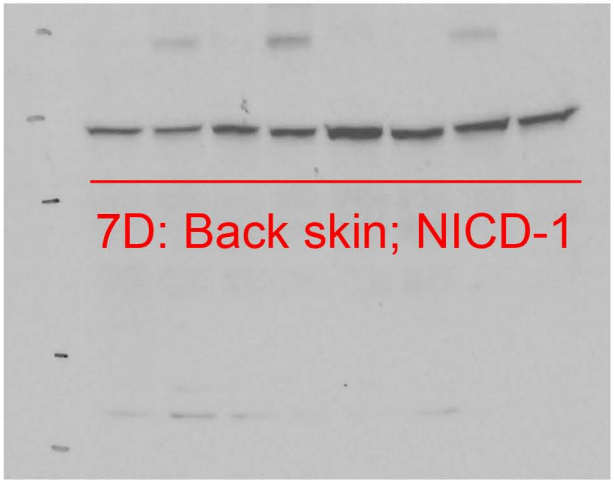

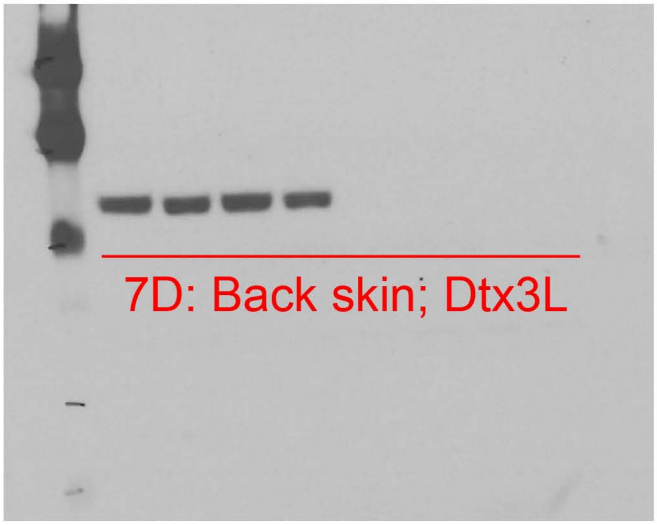

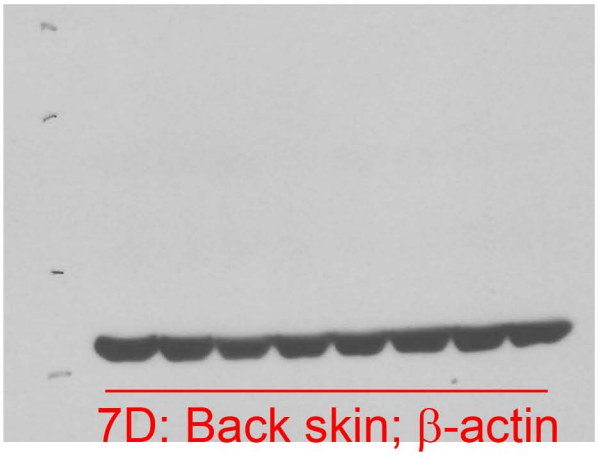

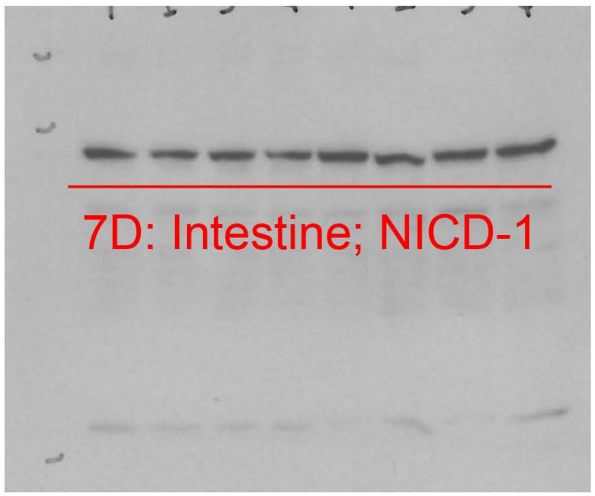

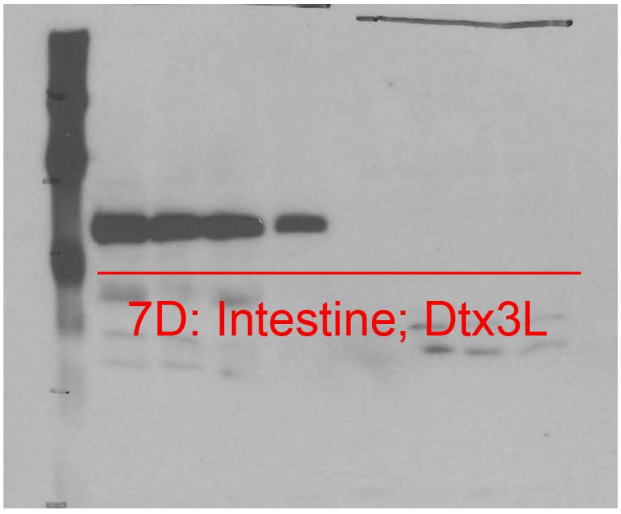

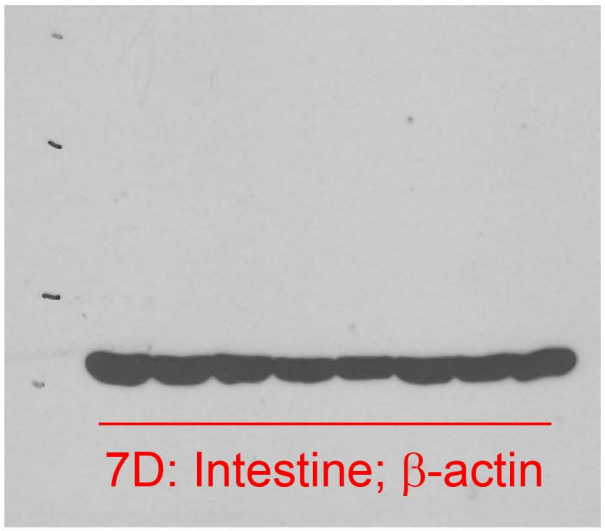

Full unedited gel for Figure 7D

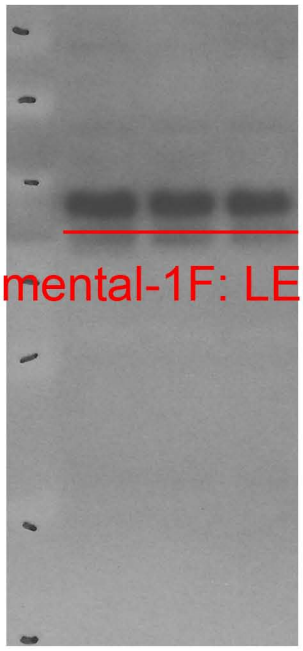

Supplemental-1F: LEC; NICD-4

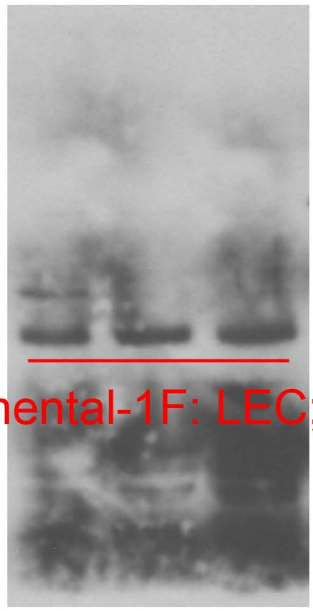

Supplemental-1F: LEC; β-actin

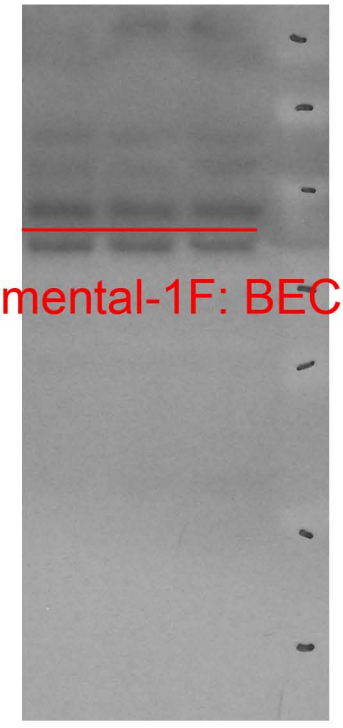

Supplemental-1F: BEC; NICD-4

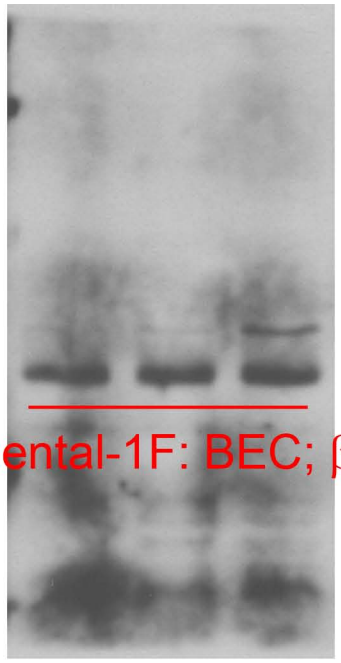

Supplemental-1F: BEC; β-actin

Full unedited gel for Supplemental Figure 1F

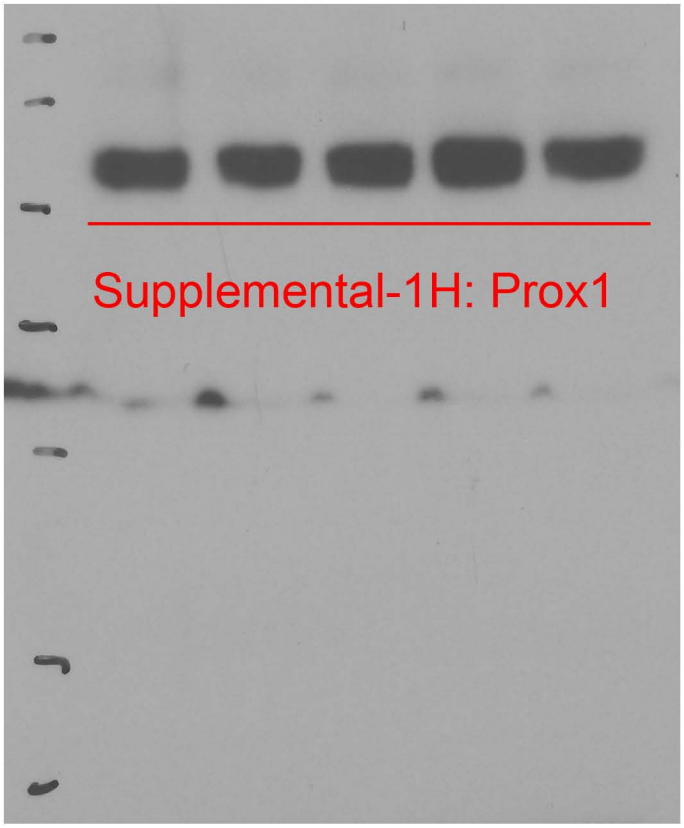

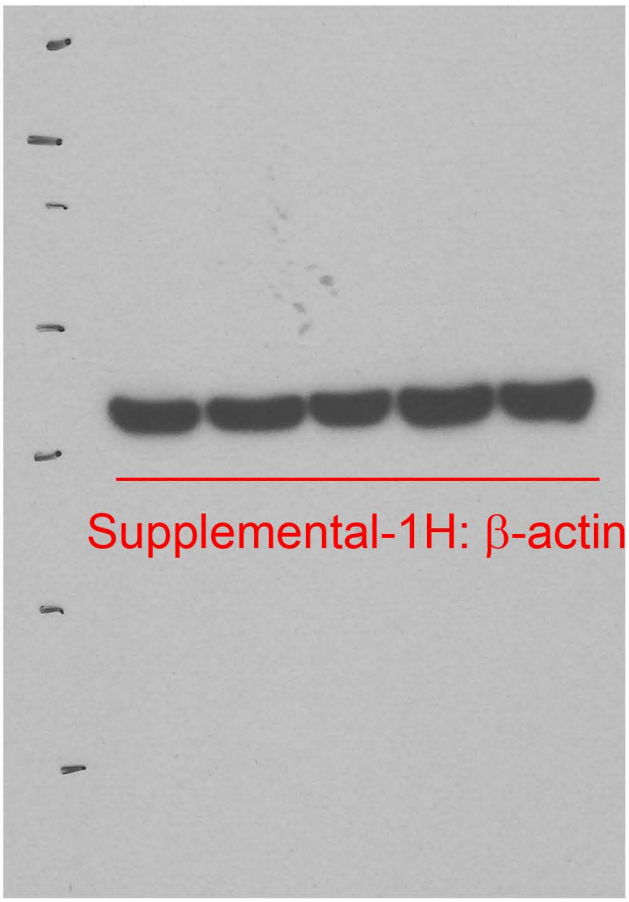

Full unedited gel for Supplemental Figure 1H

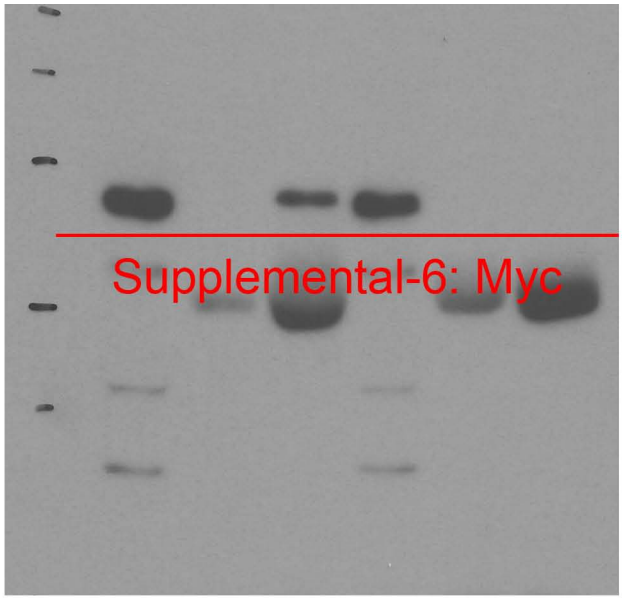

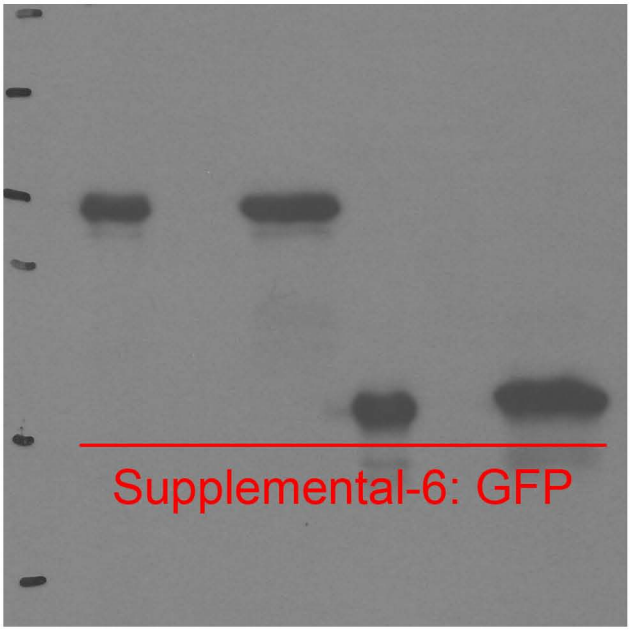

Full unedited gel for Supplemental Figure 6

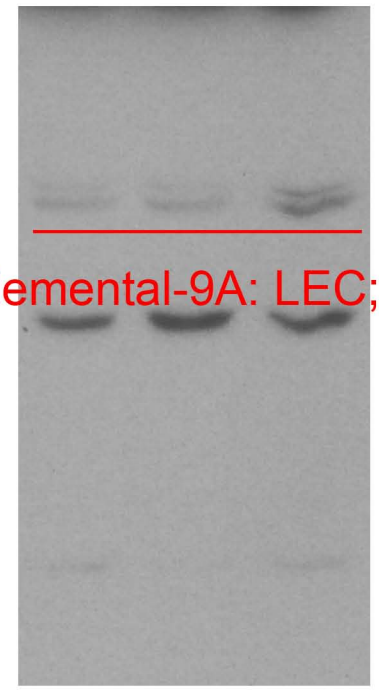

Supplemental-9A: LEC; DTX1

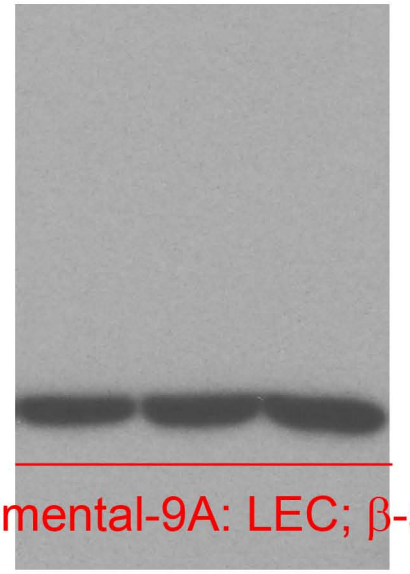

Supplemental-9A: LEC; β-actin

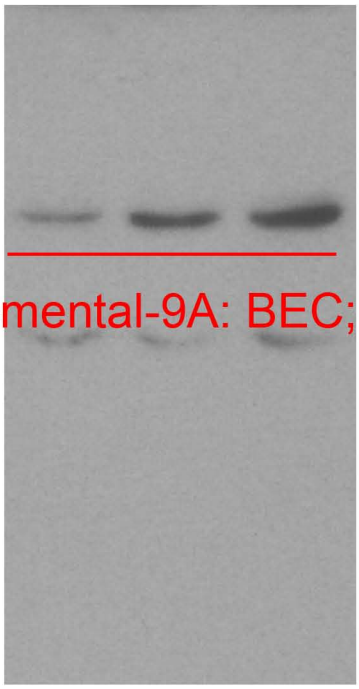

Supplemental-9A: BEC; DTX1

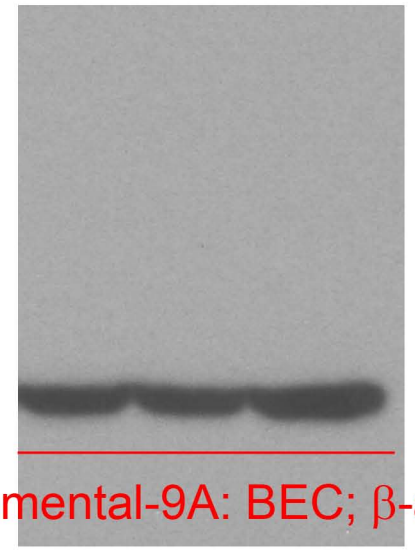

Supplemental-9A: BEC; β-actin

Full unedited gel for Supplemental Figure 9A

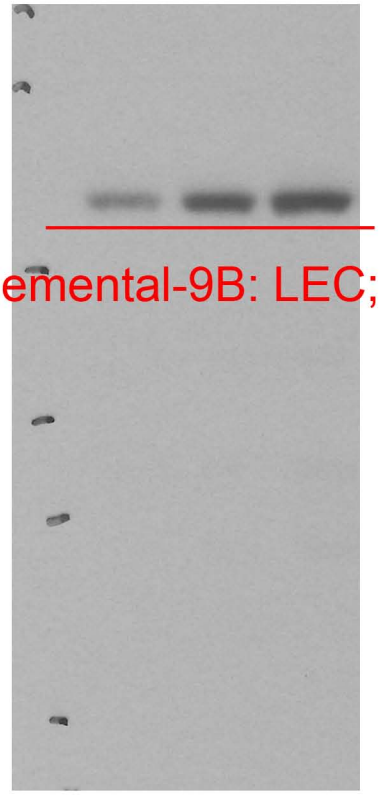

Supplemental-9B: LEC; DTX3L

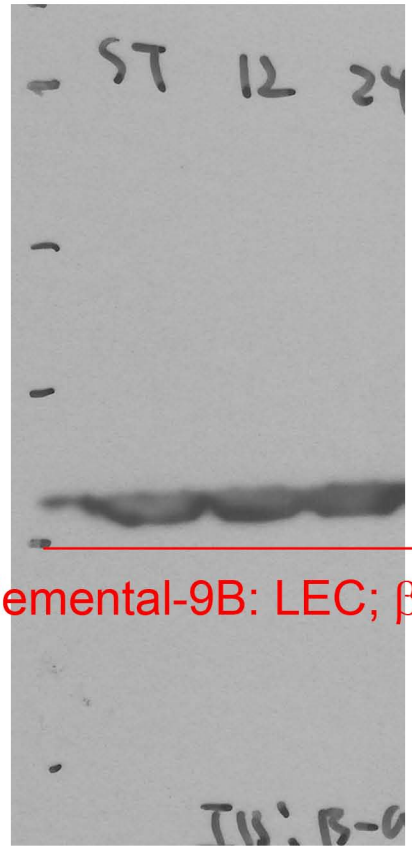

Supplemental-9B: LEC; β-actin

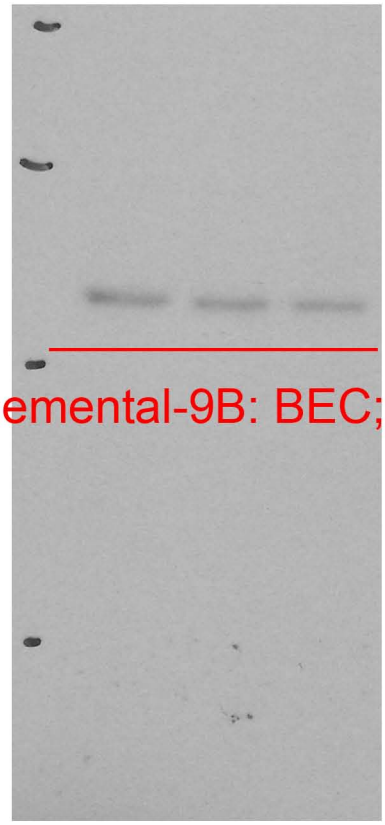

Supplemental-9B: BEC; DTX3L

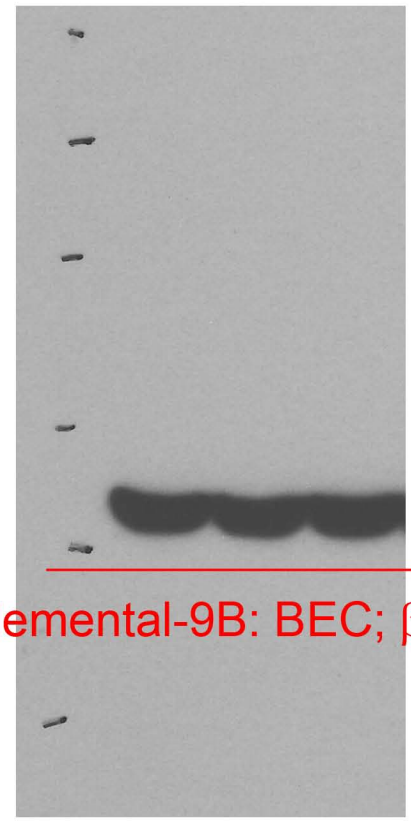

Supplemental-9B: BEC; β-actin

Full unedited gel for Supplemental Figure 9B